AFCRL-67-0129

Electromagnetic Scattering From Absorbing Spheres

Authors

George W. Kattawar and Gilbert N. Plass

Southwest Center for Advanced Studies
Dallas, Texas

Contract No. AF19(628)-5039

Project No. 4076

Task No. 407604

Scientific Report No. 1

28 December 1966

This research was partially supported by the National Aeronautics and Space Adminsitration

Contract Monitor
Robert W. Fenn

Prepared
for

AIR FORCE CAMBRIDGE RESEARCH LABORATORIES
OFFICE OF AEROSPACE RESEARCH
UNITED STATES AIR FORCE
BEDFORD, MASSACHUSETTS 01730

ELECTROMAGNETIC SCATTERING FROM ABSORBING SPHERES

by

George W. Kattawar* and Gilbert N. Plass
Southwest Center for Advanced Studies
Dallas, Texas 75230

December 28, 1966

To be Submitted to Applied Optics

This work was supported by the Air Force Cambridge Research Laboratories, Office of Aerospace Research contract AF19(628) - 5039 and by the National Aeronautics and Space Administration contract.

*George W. Kattawar is also with North Texas State University, Denton, Texas 76203.

ELECTROMAGNETIC SCATTERING FROM ABSORBING SPHERES

George W. Kattawar and Gilbert N. Plass

Abstract

A very efficient method for the calculation of Mie cross sections for absorbing particles is discussed. It is used to calculate an extensive set of curves which illustrate the dependence of the efficiency factors Q for absorption, scattering, and extinction on the size parameter x and on n_1 and n_2 (the real and imaginary parts of the index of refraction). Other curves show the height and width of the first resonance in Q_{ext} as a function of x as well as the average cosine of the scattering angle and the half-width of the angular intensity function as it depends on x, n_1, and n_2. Among the interesting features shown are the following: (1) as n_2 increases, Q_{sca} decreases to a minimum value before increasing, when $x \geq 1$ and for most values of n_1; (2) the maximum value of Q_{ext} at the first resonance decreases rapidly when a small amount of absorption is introduced; (3) over a considerable range of the parameters the width of the first resonance of Q_{ext} is proportional to n_1^{-4} when there is no absorption and to $n_2 n_1^{-2}$ when there is absorption; (4) when $n_1 >> 1$, the scattered intensity near the first resonance is predominately forward, symmetrical, or predominately backward when x is respectively somewhat smaller than, equal to, or larger than the resonance value; (5) as n_2 increases, the forward scattered intensity first increases before it decreases, when $x \geq 1$ and for most values of n_1; (6) the half-width of the angular intensity function varies as x^{-1} when $x \geq 10$ and is relatively insensitive to the value of n_1 and n_2.

George W. Kattawar is with North Texas State University, Denton, Texas, 76203 and the Southwest Center for Advanced Studies, P.O. Box 30365, Dallas, Texas 75230.

Gilbert N. Plass is with the Southwest Center for Advanced Studies, P.O. Box 30365, Dallas, Texas 75230.

Introduction

The interaction of an electromagnetic wave with an absorbing sphere is described by the Mie theory and is discussed in detail in Van de Hulst's classic book[1]. Unfortunately this book was published before the widespread use of modern computers. At that time the available results for absorbing spheres consisted of some asymptotic equations and a few isolated numerical results. Since the publication of the book, a large number of laboratories have developed computational programs applicable to the case of an absorbing sphere. However, the majority of these investigations have been concerned with a particular substance, such as water droplets (the literature on this subject has been reviewed by Deirmendjian et al[2]).

Although these calculations for particular substances are most interesting, it is difficult to gain an understanding of the behavior of the cross sections for absorbing particles from results for isolated values of the index of refraction. Aside from the general discussion in Van de Hulst's book[1], Deirmendjian et al[2], Brockes[3] and Plass[4] seem to have made the only attempts at understanding the general behavior of these cross sections.

First we present our computational scheme for the calculation of Mie cross-sections of absorbing particles. This scheme is valid for all values of the size parameter which occur in the theory regardless of whether they are very small or very large. Our scheme is both very stable numerically and is easy to program. We believe that it contains improvements over previously reported procedures.

Next, some new studies are presented of the variation of the Mie cross-sections as a functions of n_2, the complex part of the index of refraction. The efficiency factors for absorption, scattering, and extinction are shown as well as the average value of the scattering angle over a wide range of the parameters.

The efficiency factor for extinction has a resonance whose maximum value increases and whose half-width decreases as n_1, the real part of the index of refraction, increases. The variation of these quantities with both n_1 and n_2 is discussed.

The scattered intensity as a function of scattering angle decreases from its value of 0° more and more rapidly as the size parameter increases. This effect is discussed together with its dependence on both n_1 and n_2.

Computational Scheme

A computational scheme is presented in this section for the calculation of the Mie cross-sections. It is based on the Ricatti Bessel functions and appears to have some advantages over other schemes which have been described.[1-8] The basic equations can be found in many places in the literature, but their validity should be checked. We shall adopt the notation of Van de Hulst.[1] The scattering, absorption, and radiation cross-sections can be calculated from various combinations of the sum and products of the coefficients a_n and b_n*. The usual expressions for a_n and b_n are (reference 1, p. 123)

*See reference 1, p. 127-128. It should be noted that the expression for $\overline{\cos\theta}\, Q_{sca}$ is incorrect as printed. The quantities Re $(a_n a_{n+1} + b_n b_{n+1})$ and Re $(a_n b_n)$ should be replaced by Re $(a_n a_{n+1}^* + b_n b_{n+1}^*)$ and Re $(a_n b_n^*)$.

$$a_n = \frac{\psi_n'(y)\psi_n(x) - m\,\psi_n(y)\psi_n'(x)}{\psi_n'(y)\zeta_n(x) - m\,\psi_n(y)\zeta_n'(x)} \quad , \tag{1}$$

$$b_n = \frac{m\psi_n'(y)\psi_n(x) - \psi_n(y)\psi_n'(x)}{m\psi_n'(y)\zeta_n(x) - \psi_n(y)\zeta_n'(x)} \quad , \tag{2}$$

where m is the complex index of refraction, n is a positive integer, and ψ and ζ are the Ricatti Bessel functions defined by

$$\psi_n(z) = z j_n(z) = (\tfrac{1}{2}\pi z)^{\frac{1}{2}} J_{n+\frac{1}{2}}(z) \quad , \tag{3}$$

$$\zeta_n(z) = z h_n^{(2)}(z) = (\tfrac{1}{2}\pi z)^{\frac{1}{2}} H_{n+\frac{1}{2}}^{(2)}(z) \quad , \tag{4}$$

with $J_{n+\frac{1}{2}}$ and $H_{n+\frac{1}{2}}^{(2)}$ the Bessel functions of first and third kind and j_n and h_n the corresponding spherical Bessel functions. The prime denotes differentiation with respect to the argument of the function and

$$x = 2\pi a/\lambda \quad , \tag{5}$$

$$y = mx \tag{6}$$

where a is the particle radius and λ is the wavelength.

These expressions can be written in a much more convenient form for computational purposes, as was first discovered by Aden.[4] Introduce the logarithmic derivative of the Ricatti Bessel functions,

$$D_n(y) = [\ell n\ \psi_n(y)]' \quad , \tag{7}$$

$$G_n(x) = [\ell n\ \zeta_n(x)]' \quad . \tag{8}$$

Then Eqs. (1) and (2) may be rewritten after some elementary algebraic manipulation in the form

$$a_n = \frac{\psi_n(x)}{\zeta_n(x)} \left[\frac{D_n(y) - m\, D_n(x)}{D_n(y) - m\, G_n(x)} \right] , \tag{9}$$

$$b_n = \frac{\psi_n(x)}{\zeta_n(x)} \left[\frac{mD_n(y) - D_n(x)}{mD_n(y) - G_n(x)} \right] . \tag{10}$$

This is the most convenient expression for the calculation of the coefficients a_n and b_n. The expression outside the brackets involves only the ratio of Ricatti-Bessel functions of real argument. The brackets themselves depend on only two functions: (1) $G_n(x)$, where the argument is always real; (2) $D_n(y)$, where the argument may be complex. The method for the computation of these functions is discussed in the remainder of this section.

The logarithmic derivative of the Ricatti-Bessel function, D_n, satisfies the recurrence relation

$$D_{n-1}(z) = \frac{n}{z} - \frac{1}{D_n(z) + nz^{-1}} . \tag{11}$$

The function $G_n(z)$ satisfies an identical recurrence relation. These relations were first derived by Infeld[9] and have been used by several investigators. However, this relationship has always been used in the past to calculate D_n by an upward recurrence relation. Unfortunately this becomes numerically unstable when $n > |z|$, a region of particular importance for large values of x. On the other hand the downward recurrence formula for D_n is always numerically stable and is the one which should be used.

Let

$$f_n(z) = D_n(z)+\varepsilon_n(z) \quad , \tag{12}$$

where f_n is an approximate numerical value of the true value of D_n and ε_n is the error in this value. If the approximate value f_n is used in Eq. (11) in order to compute f_{n-1}, then

$$D_{n-1} + \varepsilon_{n-1} = \frac{n}{z} - \frac{1}{D_n(z)+\varepsilon_n(z)+nz^{-1}} \quad . \tag{13}$$

If D_{n-1} is replaced by its value from Eq. (11), it is found that

$$\varepsilon_{n-1} = \frac{\varepsilon_n}{(D_n+nz^{-1})\ (D_n+\varepsilon_n+nz^{-1})} \quad . \tag{14}$$

When $n>>|z|$, it follows from the series expansion of D_n that

$$D_n(z) \cong (n+1)z^{-1} \quad . \tag{15}$$

Thus,

$$|\varepsilon_{n-1}| \cong |\varepsilon_n|/|(2n+1)z^{-1}|^2 \tag{16}$$

or

$$|\varepsilon_{n-1}| << |\varepsilon_n| \quad . \tag{17}$$

Thus the computational error decreases at each step if $D_n(z)$ is calculated from Eq. (11) by downward recurrence in the order n and the calculation is started at some value $n>>|z|$. The calculations are insensitive to the assumed starting value and rapidly converge to the correct value. In practice zero is a convenient starting value for D_n.

In the regions where $n<|z|$, the function D_n becomes oscillatory and hence there is no problem in the use of the recurrence relations in this region.

Although the function G_n always has a real argument, the value of the function is complex. A similar analysis to that given above shows that an upward recurrence process may always be used with these functions. The function $G_o(x) = -i$ for all x. Thus the recurrence is always started with this remarkably simple value.

The ratio $\psi_n(x)/\zeta_n(x)$ in Eqs. (9) and (10) can be expressed in terms of $J_n(x)$ and $Y_n(x)$, the Bessel functions of first and second kind. These functions are computed from their well-known recurrence relations. J_n is computed by downward recursion and Y_n by upward recurrence, as has been discussed by several authors.[6,8]

A numerically satisfactory method has been presented in this section for the computation of all the functions which occur in Eqs. (9) and (10). This method has been tested in over a thousand cases covering a complete range of values of x and m. The results agreed in all cases with previously published results and various asymptotic equations where applicable. All calculations were performed on an IBM Model 360-50 computer using double precision arithmetic.

Cross Sections

The complex index of refraction m is the physical parameter which describes the interaction of an electromagnetic wave with an absorbing

particle. Let us write $m = n_1 - in_2$. The absorption and scattering cross sections vary with the absorbing power of the particle, which is represented mathematically by the imaginary part of the index of refraction. The variation of the cross sections as a function of n_2 has not been extensively investigated before the availability of electronic computers, because of the computational difficulties involved. Deirmendjian et al,[2] Brockes,[3] and Plass[4] have given results for particular values of n_2. Further results are given in this section which more completely illustrate the dependence of these cross sections on n_2.

In Figs. 1-3, the efficiency factor for absorption Q_{abs} (absorption cross section divided by cross-sectional area of the particle) is shown as a function of n_2 for various particular values of n_1 and x. In Fig. 1, where x = 0.1, the limiting equation

$$Q_{abs} = (\text{constant})\, n_2 \quad , \tag{18}$$

is found to be valid when $n_2 < 1$. The curves do not depend markedly on n_1 until $n_1 \geq 2$. The value of Q_{abs} decreases as n_1 increases for $n_2 < 1$.

For the intermediate value x = 1, it is seen from Fig. 2 that Eq. (1) is valid for $n_2 < 0.1$. The curves are very insensitive to the value of n_1 except near the maximum. The value of Q_{abs} first increases slightly, and then decreases, as n_1 increases, when $n_2 < 1$.

When x = 10, Fig. 3 shows that Eq. (18) is only valid for $n_2 < 0.01$. The maximum of the curves is broader than before. However, the curves are still relatively insensitive to the value of n_1 except near the maximum.

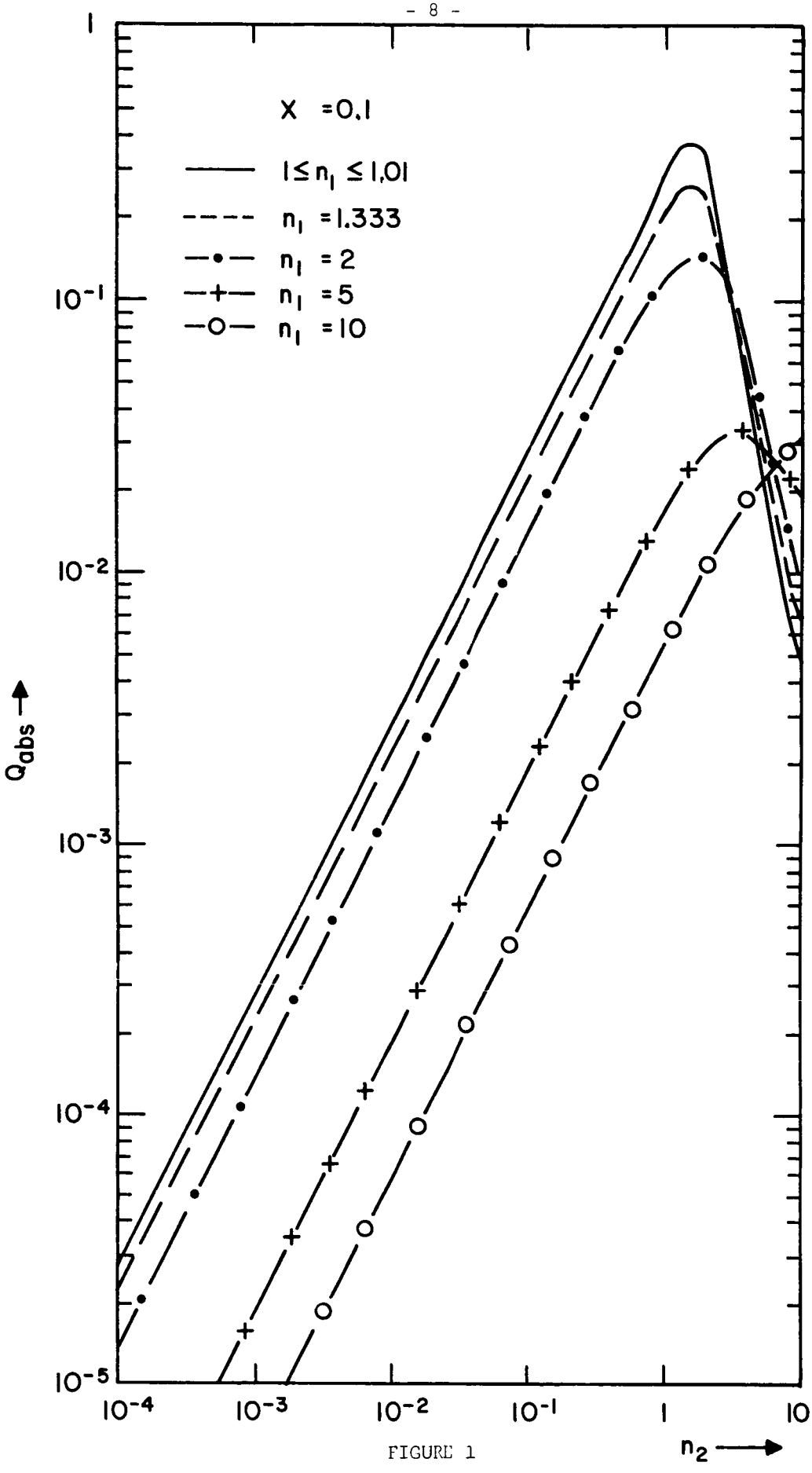
X =0.1
1≤n1≤1.01
n1 =1.333
n1 =2
n1 =5
n1 =10
Qabs
n2
1
10-1
10-2
10-3
10-4
10-5
10-4
10-3
10-2
10-1
1
10

FIGURE 1

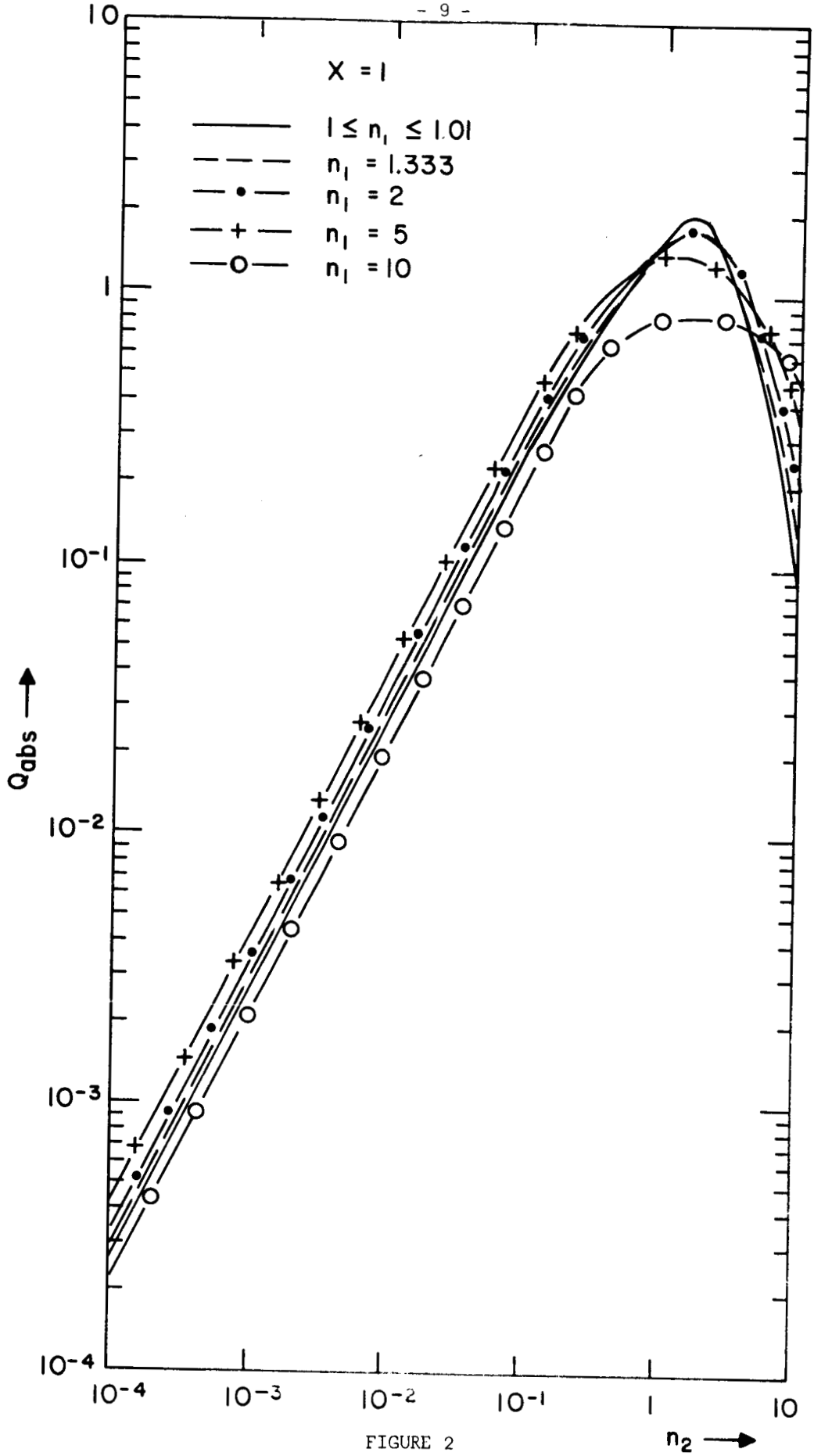
X = 1
1 ≤ n1 ≤ 1.01
n1 = 1.333
n1 = 2
n1 = 5
n1 = 10
Qabs
n2
10
1
10-1
10-2
10-3
10-4
10-4
10-3
10-2
10-1
1
10

FIGURE 2

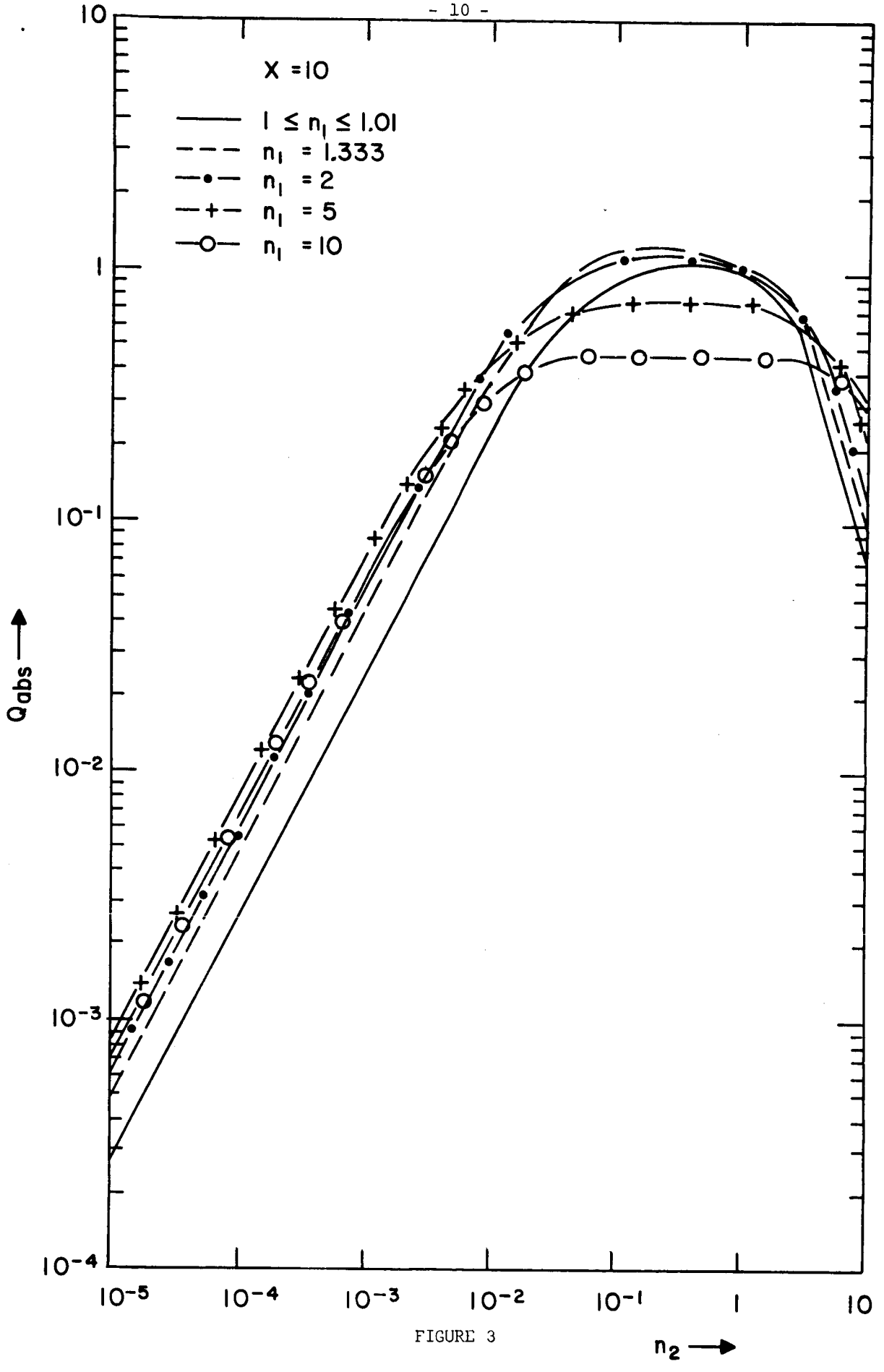
X =10
1 ≤ n1 ≤ 1.01
n1 = 1.333
n1 = 2
n1 = 5
n1 = 10
Qabs
n2
10
1
10-1
10-2
10-3
10-4
10-5
10-4
10-3
10-2
10-1
1
10

FIGURE 3

The value of Q_{abs} first increases, and then decreases, as n_1 increases, when $n_2 < 0.01$.

The efficiency factor for scattering, Q_{sca}, is shown in Figs. 4-6. Q_{sca} is independent of n_2 until n_2 exceeds some critical value. As would be expected the absorption properties of a sphere have no influence on the scattering until they are sufficiently large. When $x = 0.1$, it is seen from Fig. 4 that Q_{sca} is independent on n_2 when $n_2 < 0.01$ provided $n_1 \geq 1.333$. For very small values of n_1, such as $n_1 = 1.001$, it is found that Q_{sca} is proportional to n_2^2 over a region between the point where Q_{sca} first begins to increase and the maximum of the curve. When $n_1 \geq 5$, the curves show very little variation with n_2 over the range calculated. For small values of x, the value of Q_{sca} always increases as n_2 increases until the maximum of the curve is reached.

When $x = 1$, Fig. 5 shows that Q_{sca} is not influenced appreciably by n_2 when $n_2 \leq 10^{-2}$. However, a new feature appears in these curves. When $n_1 \geq 2$, the value of Q_{sca} first decreases as n_2 increases. It passes through a minimum value before finally increasing.

For a large value of x, such as $x \blacksquare 10$ as shown in Fig. 6, the scattering may be influenced by the absorption of the particle unless $n_2 \leq 10^{-4}$. When $n_1 \geq 1.33$, a striking feature of these curves is the very considerable decrease in Q_{sca} as n_2 increases. A minimum is reached around $n_2 = 0.1$ and then Q_{sca} increases again. A maximum in the curve may occur beyond $n_2 = 1$.

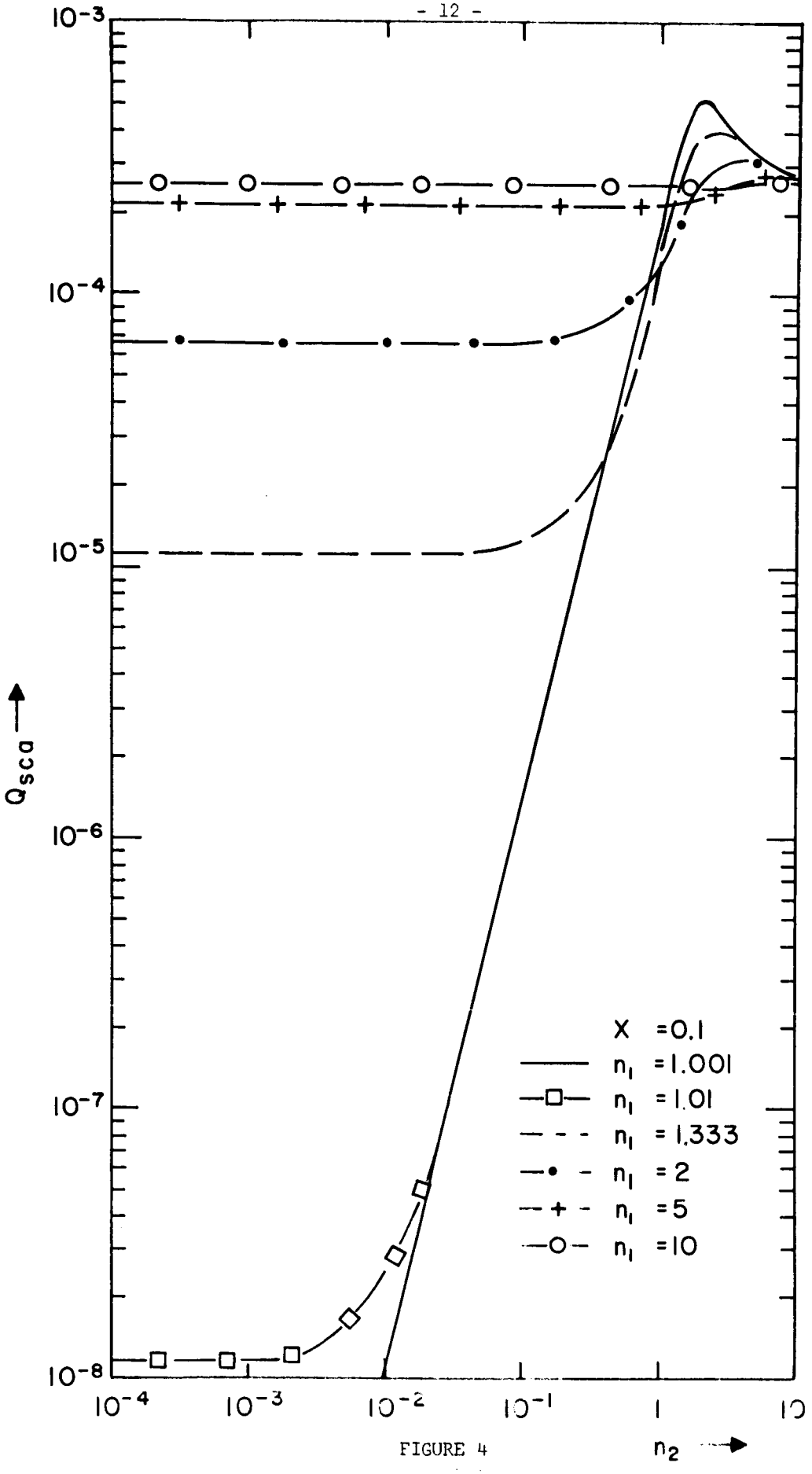
10^{-3}
10^{-4}
10^{-5}
10^{-6}
10^{-7}
10^{-8}
Q_{sca}
10^{-4}
10^{-3}
10^{-2}
10^{-1}
1
10
n_2
X =0.1
n_1 =1.001
n_1 =1.01
n_1 =1.333
n_1 =2
n_1 =5
n_1 =10

FIGURE 4

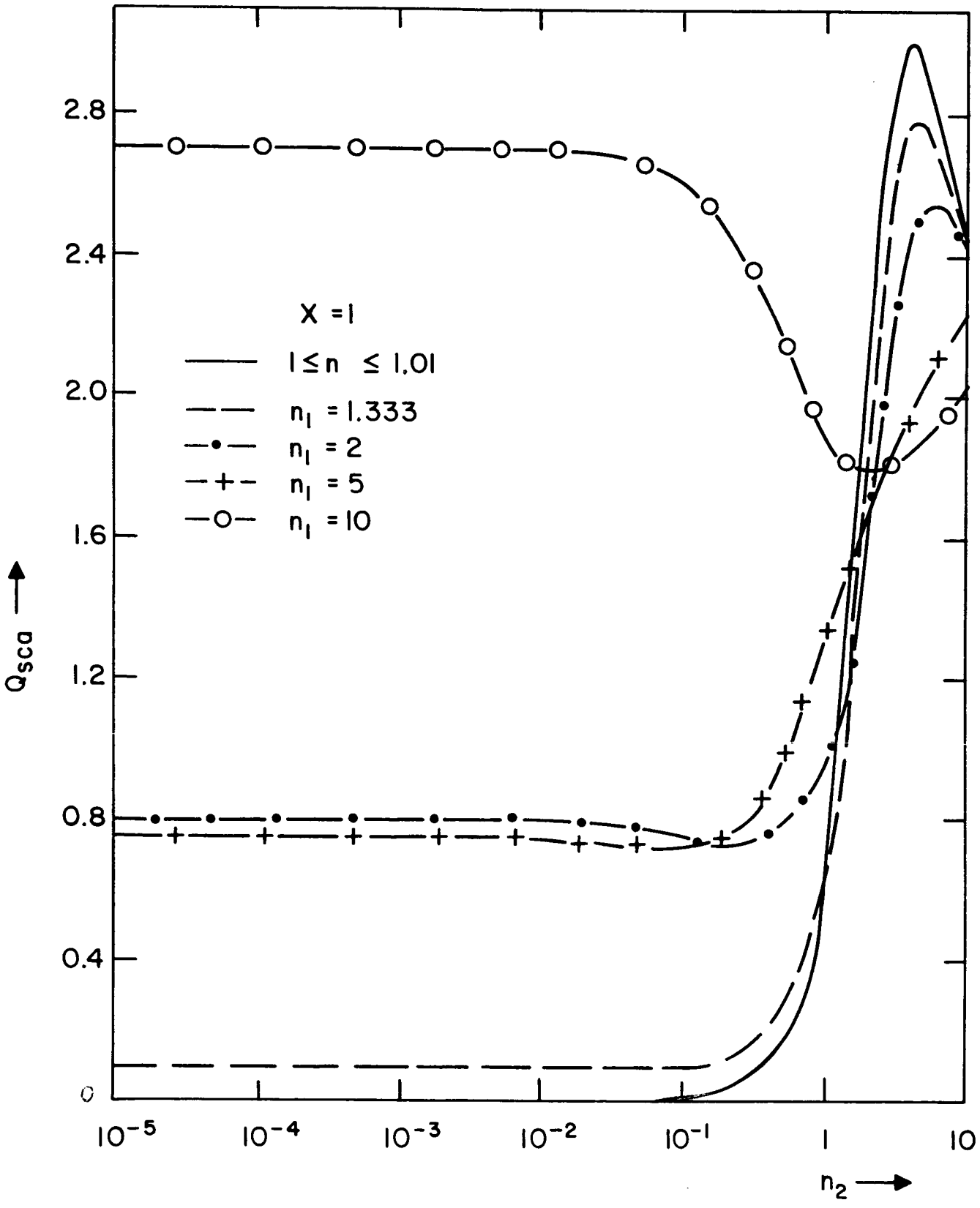
2.8
2.4
2.0
1.6
1.2
0.8
0.4
0
Q_{sca}
X = 1
1 ≤ n ≤ 1.01
n_1 = 1.333
n_1 = 2
n_1 = 5
n_1 = 10
10^{-5}
10^{-4}
10^{-3}
10^{-2}
10^{-1}
1
10
n_2

FIGURE 5

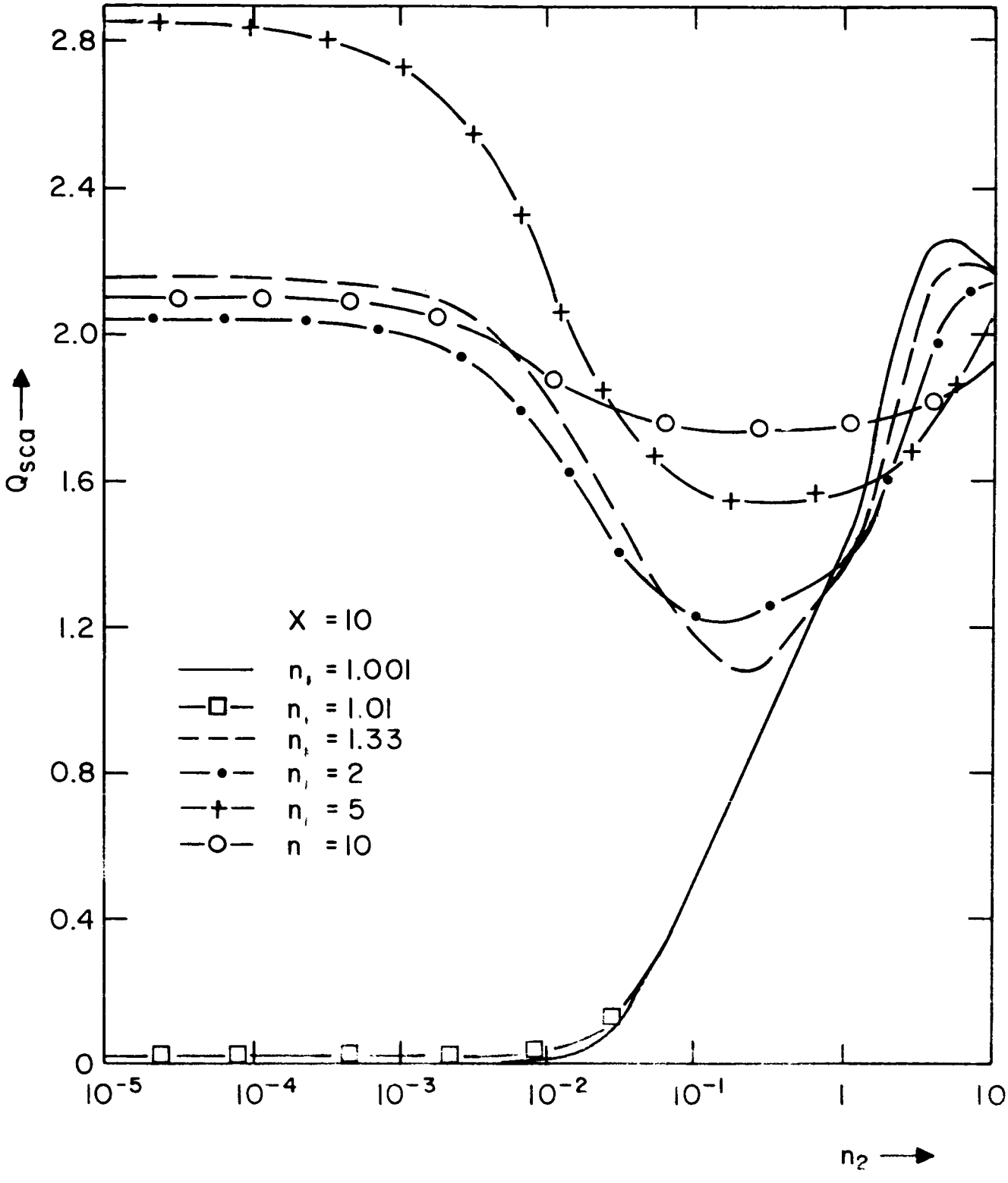
2.8
2.4
2.0
1.6
1.2
0.8
0.4
0
Q_{sca}
X = 10
n_1 = 1.001
n_1 = 1.01
n_1 = 1.33
n_1 = 2
n_1 = 5
n_1 = 10
10^{-5}
10^{-4}
10^{-3}
10^{-2}
10^{-1}
1
10
n_2

FIGURE 6

First Resonance of Extinction Cross Section

The curve of the efficiency factor for extinction as a function of the parameter x first increases from zero to a maximum value at $x_{max} = 2.05(n_1-1)^{-1}$, when $n_1 < 1.5$ and the particles are non-absorbing[1]. It is known that this first resonance becomes very narrow as n_1 increases; at the same time the value of Q_{ext} at the maximum becomes very large. The following approximate formulas are valid when n_1 is large[1].

$$x_{max} = \pi n_1^{-1} \tag{19}$$

and

$$Q_{ext,max} = 6\pi^{-2} n_1^{2}, \tag{20}$$

where x_{max} and $Q_{ext,max}$ are the values of x and Q_{ext} at the maximum. The above approximate equations are valid only for real values of m. The behavior of this resonance when the particles are absorbing has not been reported, except for the case $n_1 = 50$ (Fig. 18, reference 3). The present code was used to calculate the values at the maximum; a special code was developed which calculated the total width of the resonance at half maximum.

The calculated values of x_{max} are compared in Table I with those obtained from the approximate Eq. (19). The values obtained from Eq. (19) are always too high, but approach the correct value more closely as n_1 increases. The position of the maximum is amazingly insensitive to the value of n_2; the value of x_{max} increases slightly as n_2 increases.

Table I. Value of x at first resonance

n_1	n_2	x_{max} calculated from exact equations	x_{max} from Eq. (19)
5	0	0.6106	0.6283
5	0.1	.6109	
5	1	.6279	
10	0	.3113	.3142
10	0.1	.3114	
10	1	.3115	
20	0	.156696	.157080
20	0.1	.156706	
20	1	.156725	
50	0	.062807	.062832
50	0.1	.062808	
50	1	.062819	
70	0	.044871	.044880
70	0.1	.044871	
70	1	.044877	
100	0	.031413	.031416
100	0.1	.031413	
100	1	.031414	

The value of Q_{ext} at the first maximum is shown in Fig. 7 as a function of n_1. The approximate Eq. (20) is quite accurate for non-absorbing particles when $n_1 > 10$. The maximum value of Q_{ext} increases as n_1^2. However, the value at this resonance is greatly reduced when the particles are even slightly absorbing. For a particular value of n_2, the value of Q_{ext} at the first resonance approaches a limiting value as n_1 increases.

The total width of the first resonance at half maximum was calculated by a computer routine which searched for the x values on both sides of the resonance which had Q_{ext} equal to one-half the value at the maximum. This resonance becomes very sharp as n_1 increases and the half-width becomes correspondingly small. The width at half-maximum is shown in Fig. 8 as a function of n_1. When $n_2 = 0$, the half-width decreases as n_1^{-4}. When $n_1 = 100$, the half-width is $2.1\ (10)^{-7}$ compared to the value of x at the resonance of $3.14\ (10)^{-2}$. On the other hand the half-width is much larger when the particle has any appreciable absorption. As shown in Fig. 8, there is a region in the upper right part of the diagram where the half-width for absorbing spheres is proportional to n_2 and n_1^{-2}. The ability of a relatively small amount of absorption both to broaden the resonance and to reduce its peak value is very striking.

Influence of Absorption on Angular Distribution

The variation of the angular distribution for the scattered intensity has been given by Plass[4] for some particular cases over a wide range of

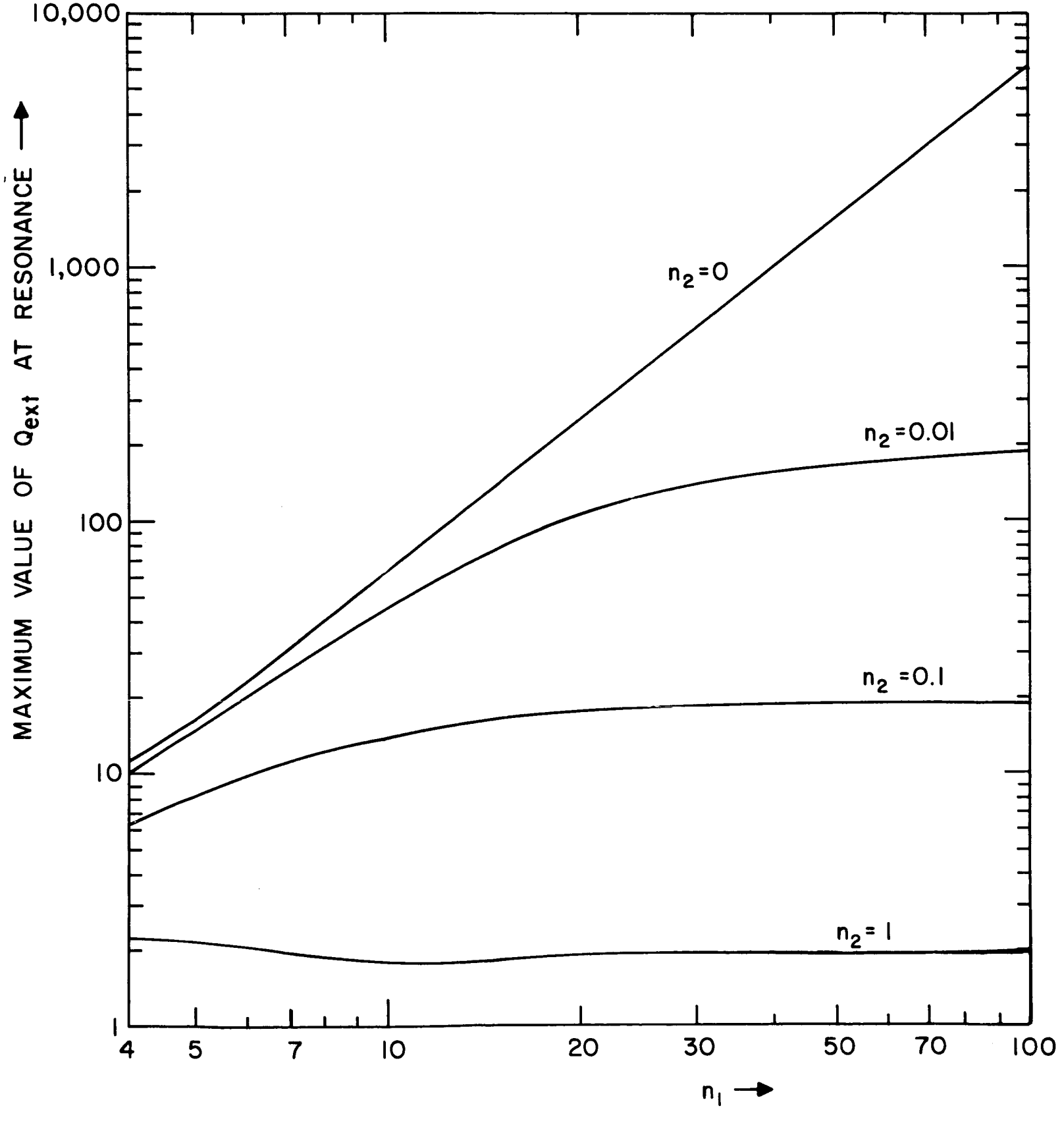
10,000
1,000
100
10
1
MAXIMUM VALUE OF Q_{ext} AT RESONANCE
$n_2=0$
$n_2=0.01$
$n_2=0.1$
$n_2=1$
4
5
7
10
20
30
50
70
100
n_1

FIGURE 7

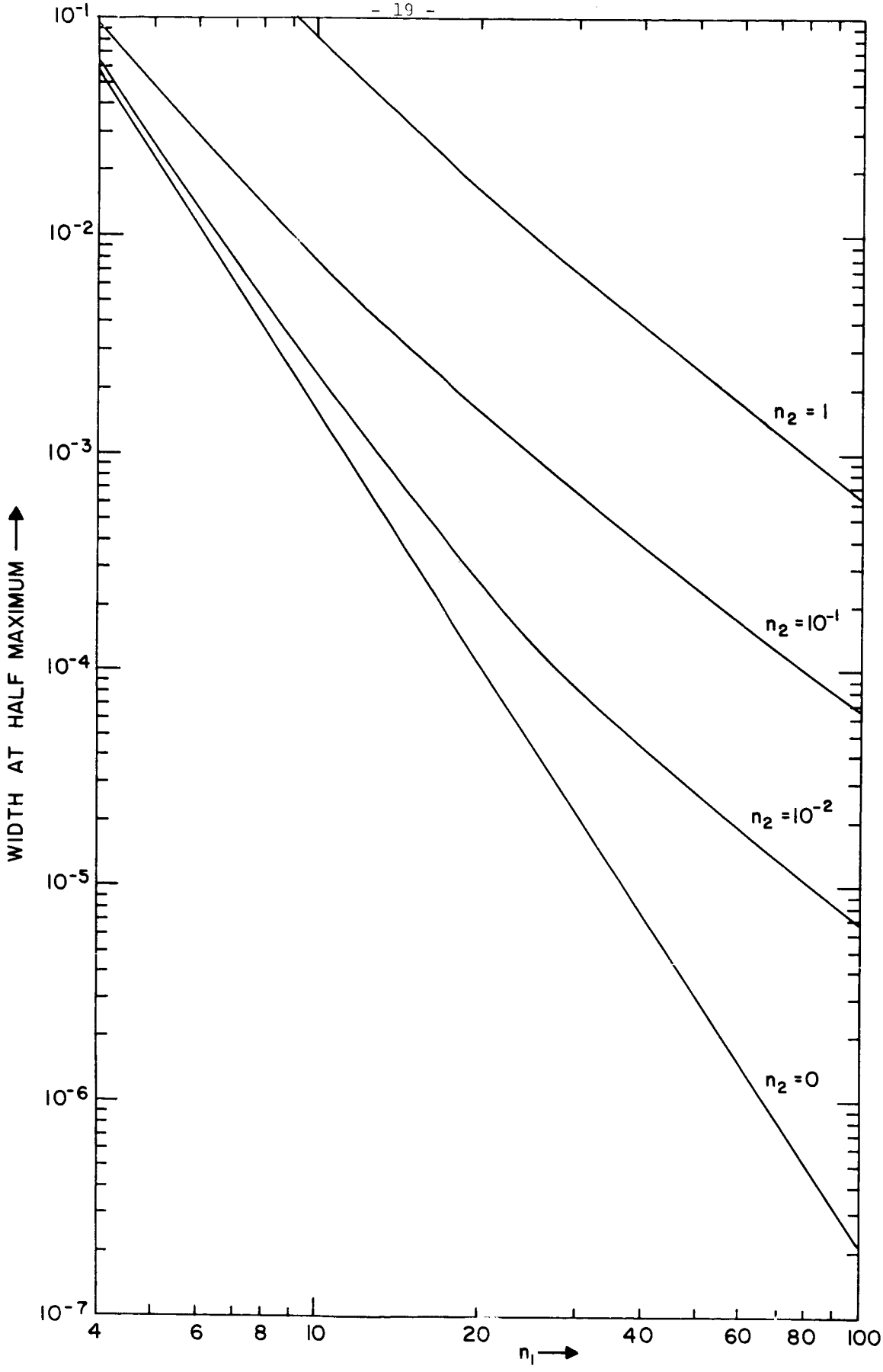
WIDTH AT HALF MAXIMUM
10^{-1}
10^{-2}
10^{-3}
10^{-4}
10^{-5}
10^{-6}
10^{-7}
$n_2 = 1$
$n_2 = 10^{-1}$
$n_2 = 10^{-2}$
$n_2 = 0$
4
6
8
10
20
40
60
80
100
n_1

FIGURE 8

values of n_2 when $x = 1$, 5, and 8. The average value of the cosine of the scattering angle over both directions of polarization (as defined by Van de Hulst , p. 128) contains a considerable amount of information about the predominant scattering directions in a single numerical value. It then becomes possible to present this information in graphical form for a wide range of values of the other parameters of the problem.

In Figs. 9-11 the average value of the cosine of the scattering angle is given as a function of n_2. The curves in Fig. 9 are for $x = 0.1$. For this small value of x, the scattering is given closely by the Rayleigh scattering function which is symmetric about $\theta = 90°$. For $n_2 \leq 0.1$, the average scattering angle is slightly in the forward direction; the average value of the cosine, $\langle \cos \theta \rangle_{av}$, is around 0.002. Thus, $\langle \theta \rangle_{av}$ is of the order $\frac{1}{2}\pi$ - 0.002 radians. The angular distribution is not appreciably influenced by the absorption of the spherical particle until n_2 is of the order of unity. Then the scattering distribution changes rapidly as n_2 increases still further; the $\langle \cos \theta \rangle_{av}$ becomes negative, which indicates a slight preponderance of backward scattering when n_2 is large. For example, $\langle \cos \theta \rangle_{av} = -0.0287$ when $n_1 = 1.33$ and $n_2 = 10$.

The curves in Fig. 10 for $x = 1$ exhibit a considerably more complex behavior. In the first place the value of $\langle \cos \theta \rangle_{av}$ in the limit of small absorption depends on the value of n_1; it is positive when $n_1 \leq 2$ ($\langle \theta \rangle_{av} = 1.29$ radians or 74° when $n_1 = 2$) and negative when $n_1 = 5$ and 10 ($\langle \theta \rangle_{av} = 1.60$ radians or 103° when $n_1 = 5$). The angular distribution is

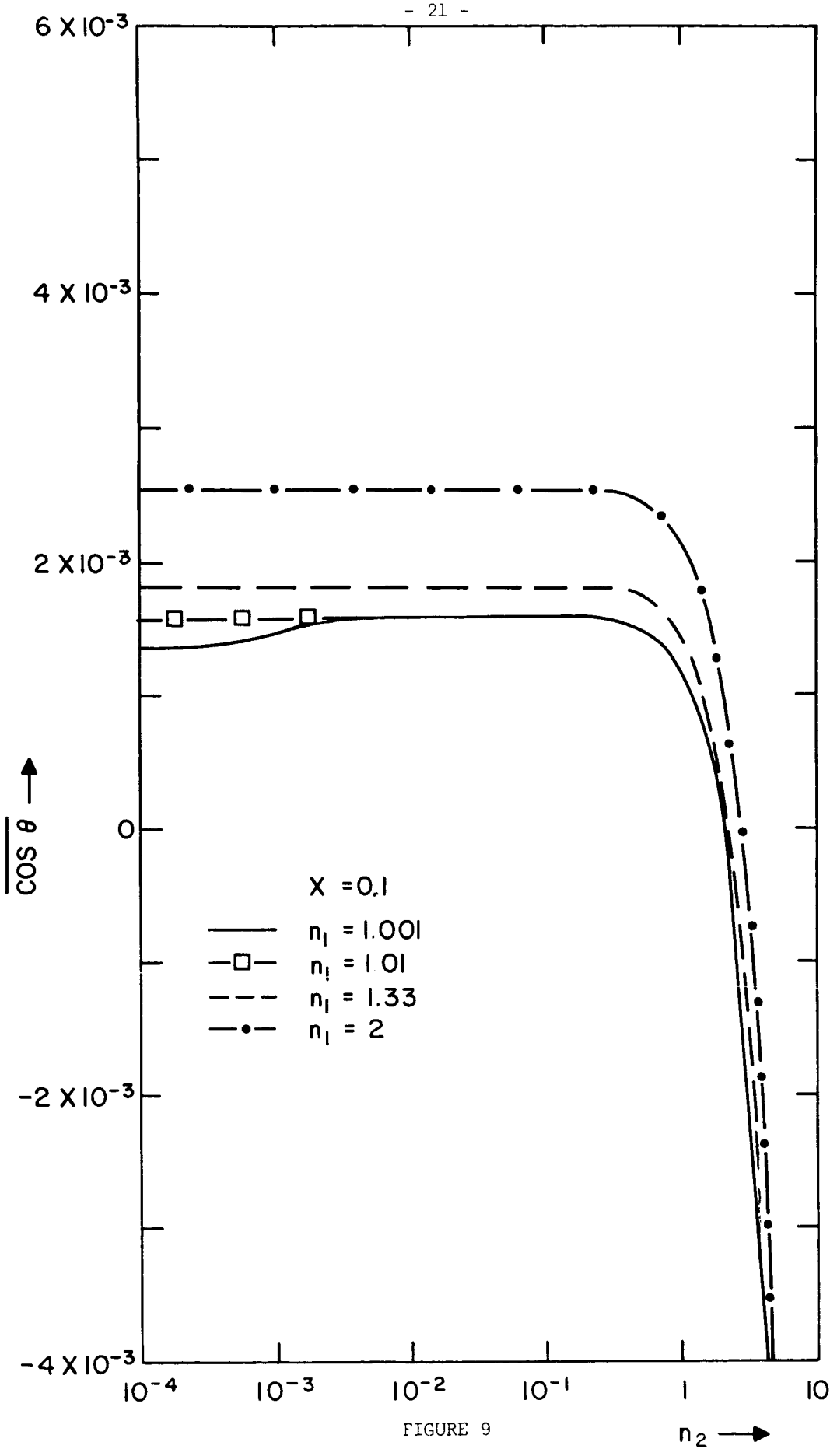
6 X 10⁻³
4 X 10⁻³
2 X 10⁻³
0
-2 X 10⁻³
-4 X 10⁻³
COS θ
X = 0.1
n₁ = 1.001
n₁ = 1.01
n₁ = 1.33
n₁ = 2
10⁻⁴
10⁻³
10⁻²
10⁻¹
1
10
n₂

FIGURE 9

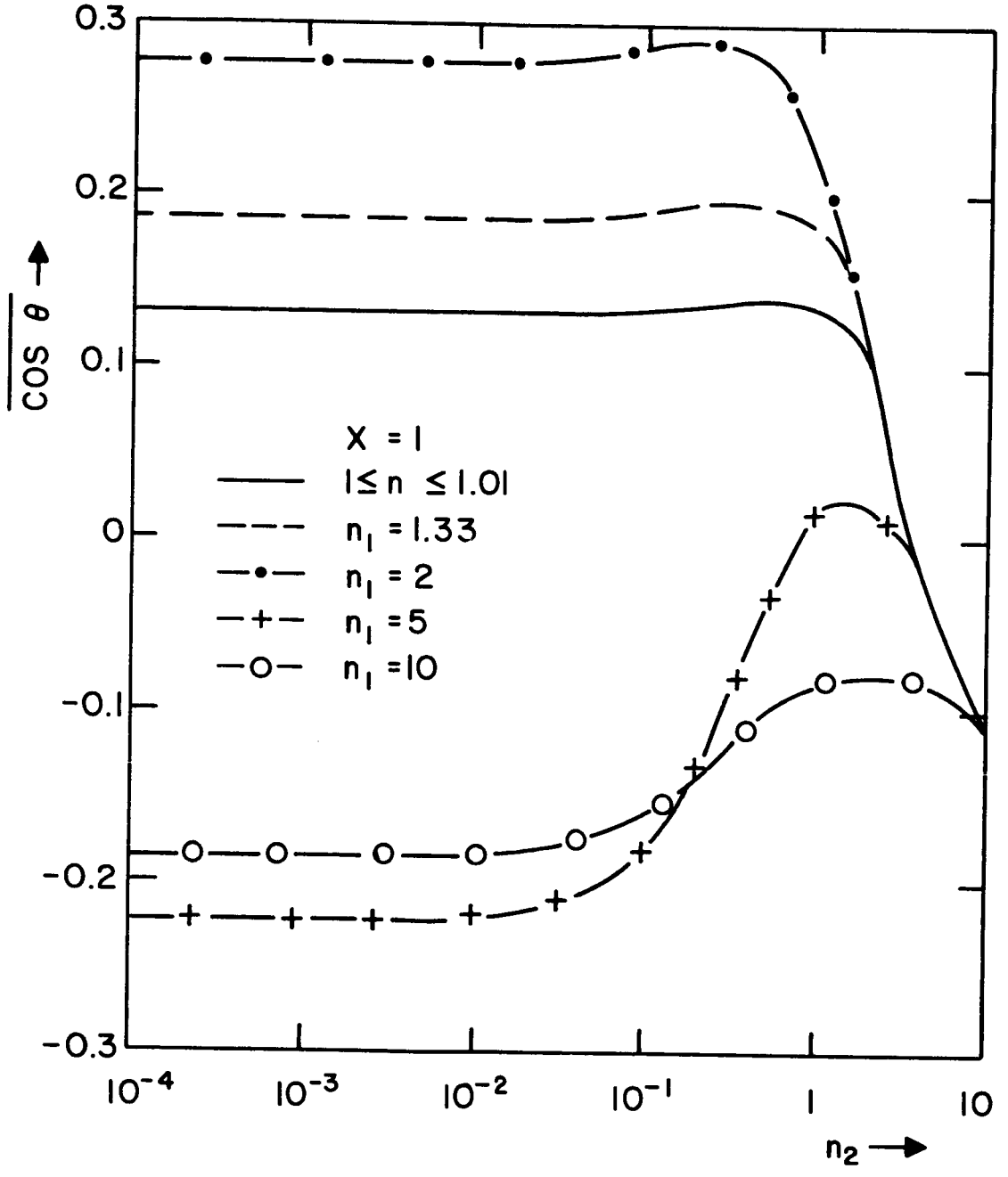
0.3
0.2
0.1
0
-0.1
-0.2
-0.3
$\overline{\cos\theta}$
X = 1
1≤ n ≤1.01
n_1 = 1.33
n_1 = 2
n_1 = 5
n_1 = 10
10^{-4}
10^{-3}
10^{-2}
10^{-1}
1
10
n_2

FIGURE 10

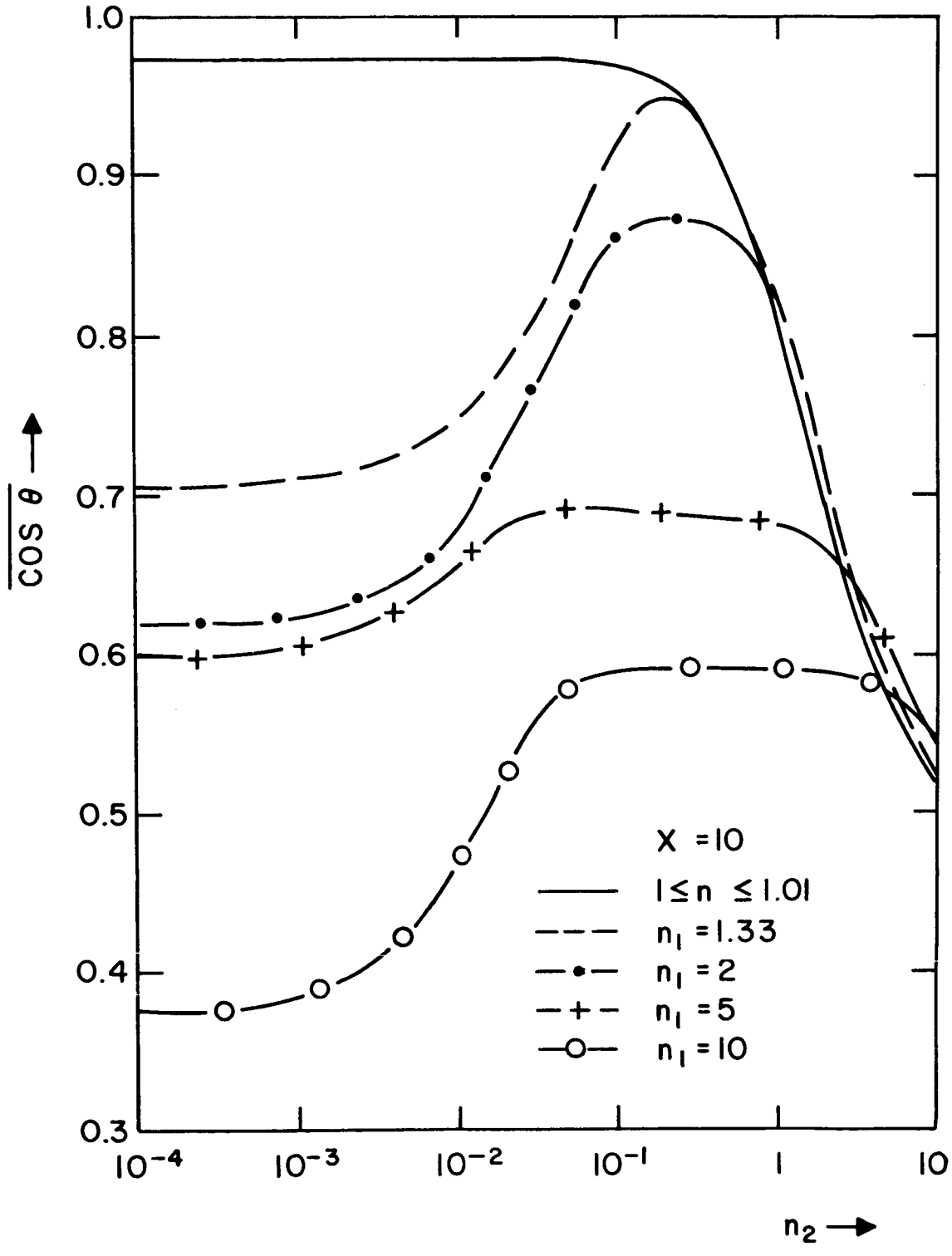
1.0
0.9
0.8
0.7
0.6
0.5
0.4
0.3
$\overline{\cos\theta}$ →
10^{-4}
10^{-3}
10^{-2}
10^{-1}
1
10
n_2 →
X = 10
1 ≤ n ≤ 1.01
n_1 = 1.33
n_1 = 2
n_1 = 5
n_1 = 10

FIGURE 11

first influenced by n_2 at a value of approximately 0.01; $\langle \cos \theta \rangle_{av}$ increases to a maximum value and then decreases again as n_2 increases. The value of $\langle \cos \theta \rangle_{av}$ is positive for $n_1 = 5$ over a narrow range near $n_2 = 1$. When $n_2 >> 1$, $\langle \cos \theta \rangle_{av}$ is negative. It is interesting to compare these curves for $n_1 = 1.33$ with Fig. 16 of reference 3.

The curves for $x = 10$ are shown in Fig. 11. For large values of x the scattering is strongly forward; thus all values of $\langle \cos \theta \rangle_{av}$ shown in this figure are positive. For small values of n_2, $\langle \theta \rangle_{av} = 0.238$ radians or approximately 14° when $n_1 \leq 1.01$. As n_2 increases all of the curves for $n_1 \geq 1.33$ pass through a broad maximum and then decrease. The maximum forward scattering usually occurs for n_2 in the range from 0.1 to 1 (compare with Fig. 17 of reference 3). Except for very small values of n_1, the forward scattering is less pronounced for weakly absorbing spheres. It is instructive to compare these results with the very interesting curves of Irvine.[10]

Angular Distribution Near a Resonance

The angular distribution exhibits an anomalous behavior near the resonances of Q_{ext}. This is illustrated in Figs. 12-14 when $n_1 = 10$, $n_2 = 0$. For comparison purposes Q_{ext} is also plotted in Figs. 12 and 13. The values of x at the resonances shown on these figures are given in Table II together with the maximum value of Q_{ext} at each resonance.

For small values of x the scattering might be expected to follow the Rayleigh distribution and to be symmetric around 90°. The actual scattering

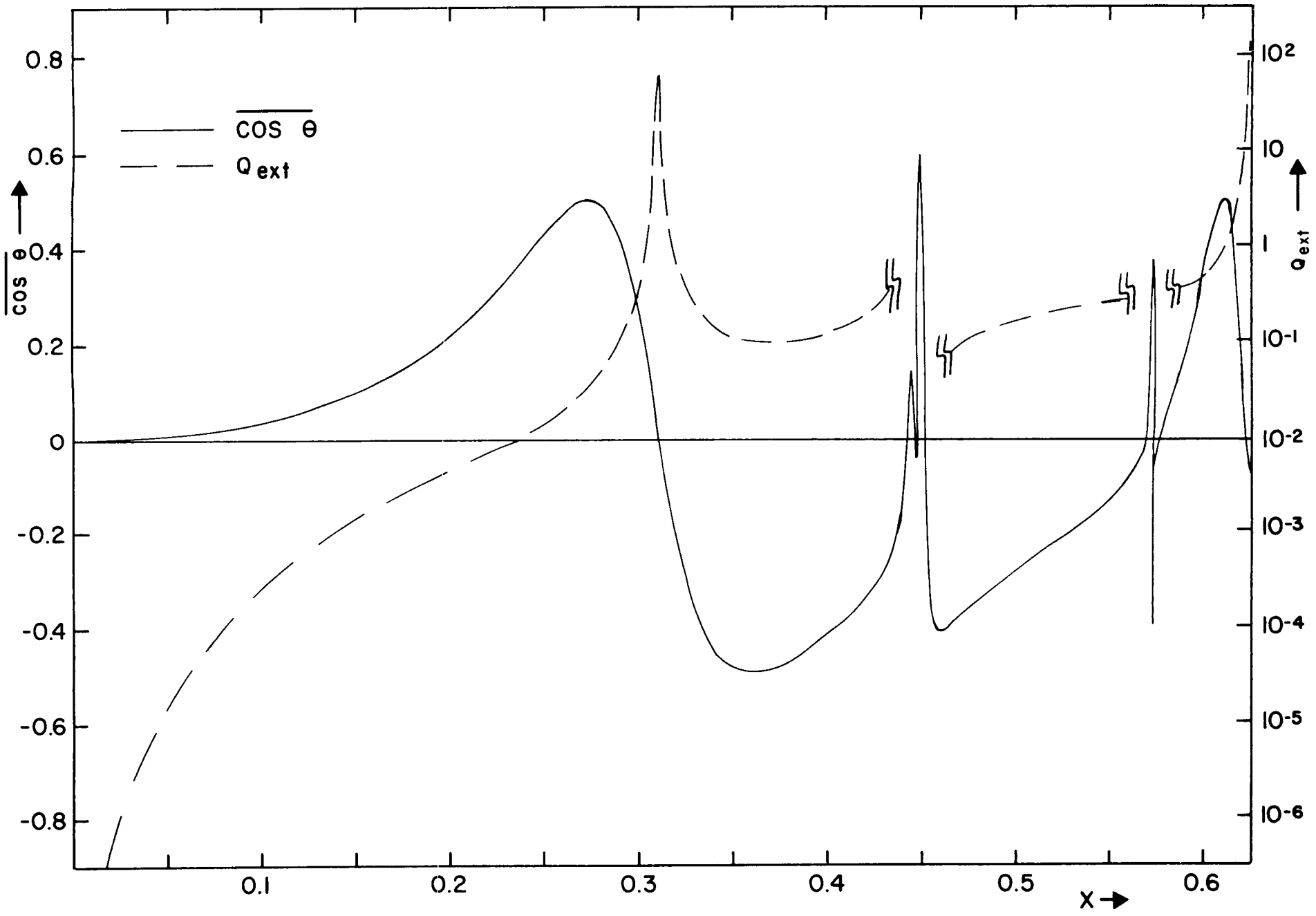
0.8
0.6
0.4
0.2
0
-0.2
-0.4
-0.6
-0.8
$\overline{\cos\theta}$
Q_{ext}
10^2
10
1
10^{-1}
10^{-2}
10^{-3}
10^{-4}
10^{-5}
10^{-6}
0.1
0.2
0.3
0.4
0.5
0.6
X

FIGURE 12

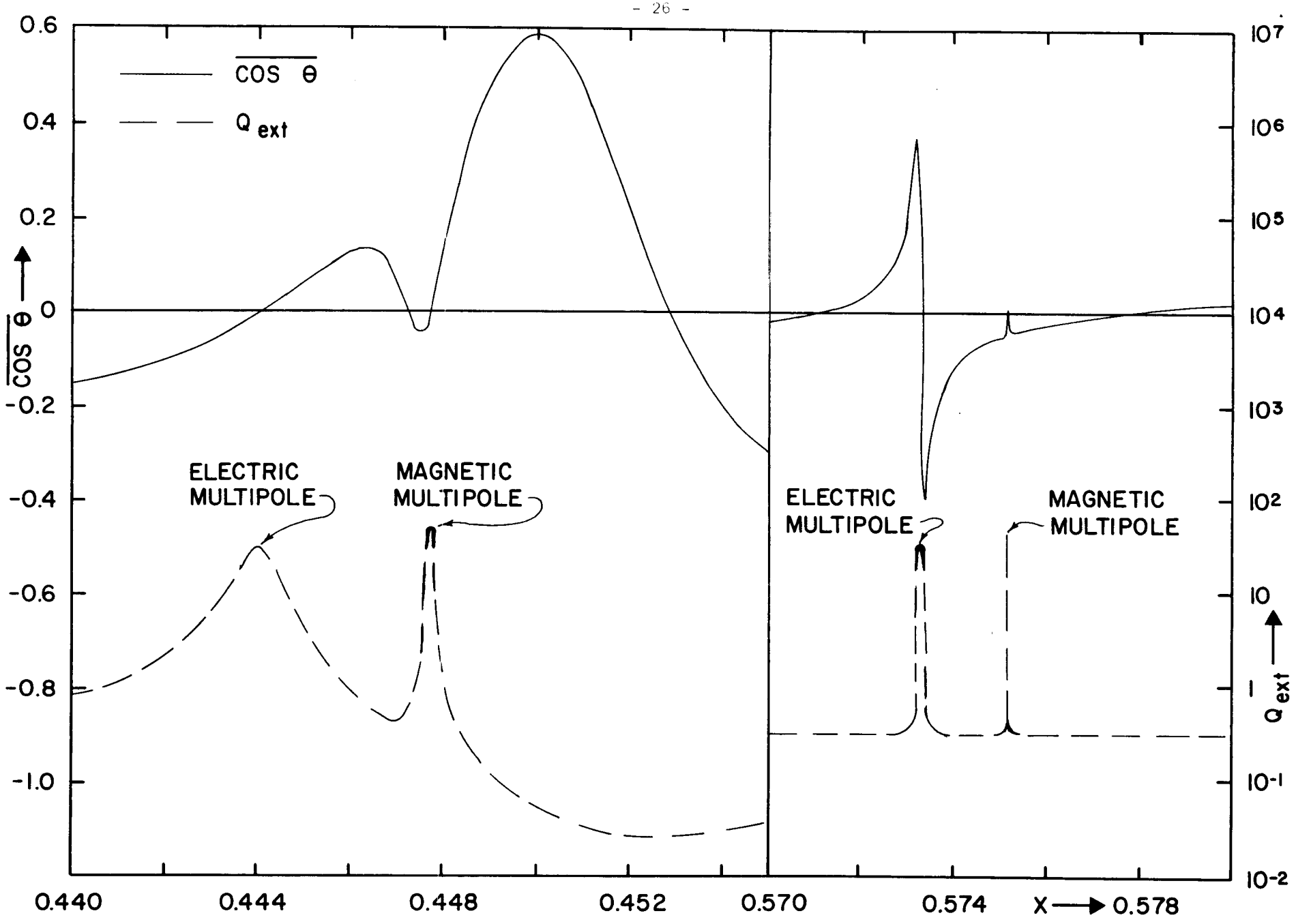
0.6
0.4
0.2
0
-0.2
-0.4
-0.6
-0.8
-1.0
$\overline{\cos\theta}$
$\overline{\cos\theta}$
Q_{ext}
ELECTRIC MULTIPOLE
MAGNETIC MULTIPOLE
ELECTRIC MULTIPOLE
MAGNETIC MULTIPOLE
10^7
10^6
10^5
10^4
10^3
10^2
10
1
10^{-1}
10^{-2}
Q_{ext}
0.440
0.444
0.448
0.452
0.570
0.574
X → 0.578

FIGURE 13

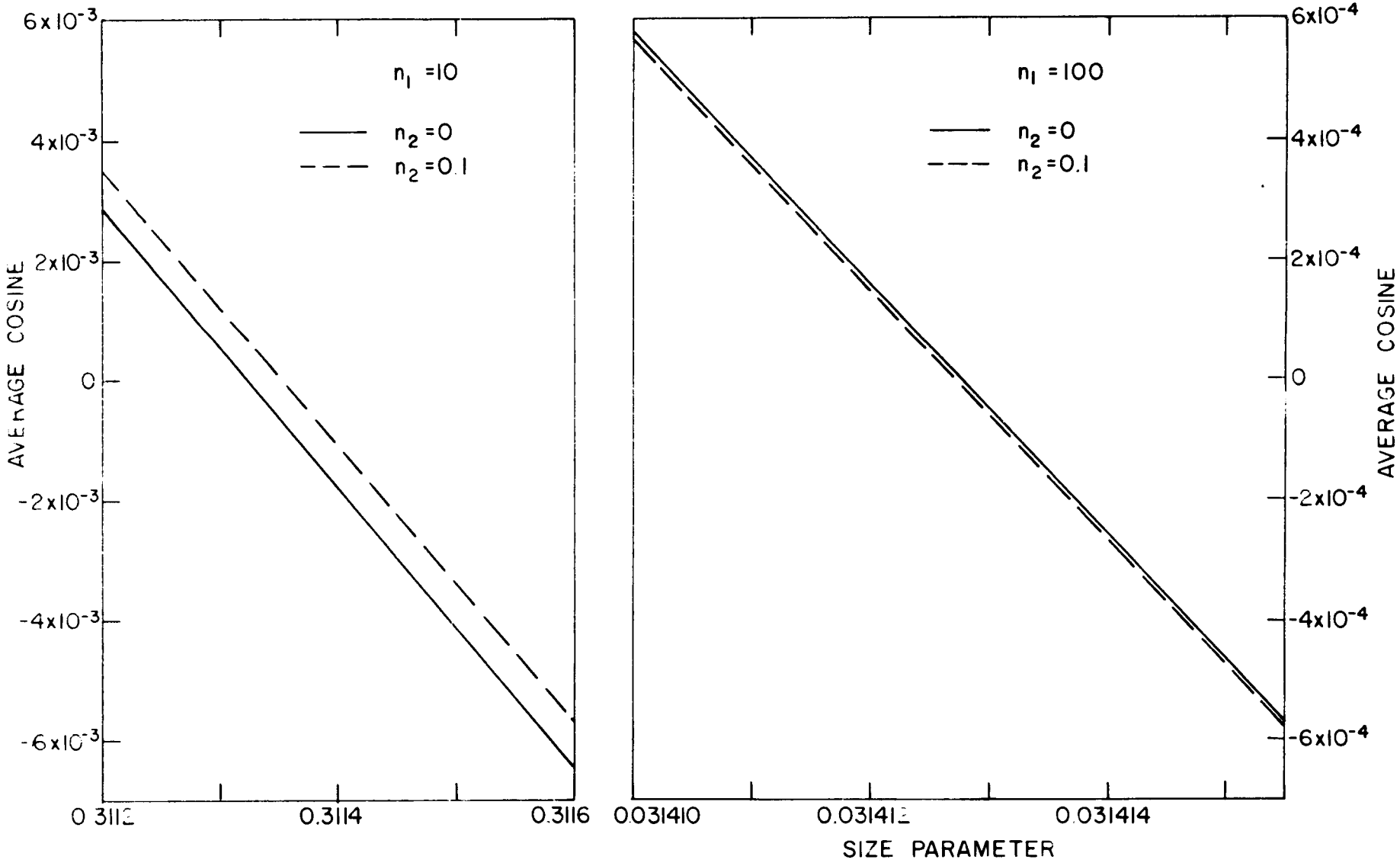
6x10-3
4x10-3
2x10-3
0
-2x10-3
-4x10-3
-6x10-3
AVERAGE COSINE
n1 =10
n2 =0
n2 =0.1
0.3112
0.3114
0.3116
n1 =100
n2 =0
n2 =0.1
6x10-4
4x10-4
2x10-4
0
-2x10-4
-4x10-4
-6x10-4
AVERAGE COSINE
0.031410
0.031412
0.031414
SIZE PARAMETER

FIGURE 14

Table II. Value of x and Q_{ext} at resonance for $n_1 = 10$, $n_2 = 0$.

Value of n (see Eqs. (1) and (2))	Type of multipole	x	Q_{ext}
1	magnetic	0.31131	61.9
1	electric	0.44404	30.5
2	magnetic	0.44775	50.0
2	electric	0.57330	30.7
3	magnetic	0.57516	42.3

pattern is very far from this simple distribution. The value of $\langle \cos \theta \rangle_{av}$ is small when $x < 0.1$. However as shown in Fig. 12, as x increases toward the first resonance, $\langle \cos \theta \rangle_{av}$ increases to a maximum value of 0.50 at $x = 0.275$. Its value then decreases rapidly and passes through zero at nearly the same value of x at which the resonance occurs. The value of $\langle \cos \theta \rangle_{av}$ then becomes increasingly negative and reaches a minimum at $x = 0.360$ when $\langle \cos \theta \rangle_{av} = -0.50$.

The same type of behavior occurs at each of the higher multipole resonances as is shown in more detail in Fig. 13. At each resonance $\langle \cos \theta \rangle_{av}$ passes through zero at nearly the resonance point. For values of x slightly smaller than the magnetic dipole resonance (n = 1), the scattering is predominately forward; for the higher magnetic multipoles, the scattering as influenced by the resonance is predominately backward for n = 2 and forward for n = 3 (where the interaction is not sufficiently strong to entirely alter the general trend of the curve) when x is

slightly smaller than the resonance value. Similarly for the electric multipoles when x is slightly smaller than the resonance value, the scattering is predominately backward for n = 1 and forward for n = 2. The influence of the multipole resonance on the scattering oscillates in this manner as each higher resonance is encountered.

The electric and magnetic multipole resonances tend to occur in closely spaced pairs. As the order of the multipole increases these pairs tend to become closer together and the resonances become sharper. The magnitude of Q_{ext} for both the magnetic and electric multipole resonances are predicted quite closely by the approximate equation given on p. 157 of Van de Hulst[1].

The value of $\langle \cos \theta \rangle_{av}$ in the immediate vicinity of the first resonance is shown in Fig. 14 for n_1 = 10 and 100 and n_2 = 0 and 0.1. This figure shows in more detail that $\langle \cos \theta \rangle_{av}$ is zero at a value of x that is extremely close to the resonance value for x. These curves are only very slightly influenced by the value of n_2. The values of $\langle \cos \theta \rangle_{av}$ for n_1 = 100 are the same as those for n_1 = 10 on the scale of Fig. 12 up to x = 0.4 (except for some very minor variations such as crossing the axis at the first resonance at a slightly larger x value), provided the x values for n_1 = 100 are multiplied by 10 before comparison.

The angular intensity patterns are so unusual near a resonance that three examples of the complete patterns are given in Fig 15 for n_1 = 10, n_2 = 0. The values of x chosen for this graph (x = 0.275, 0.31131, 0.360) correspond to the maximum forward scattering, scattering at the resonance

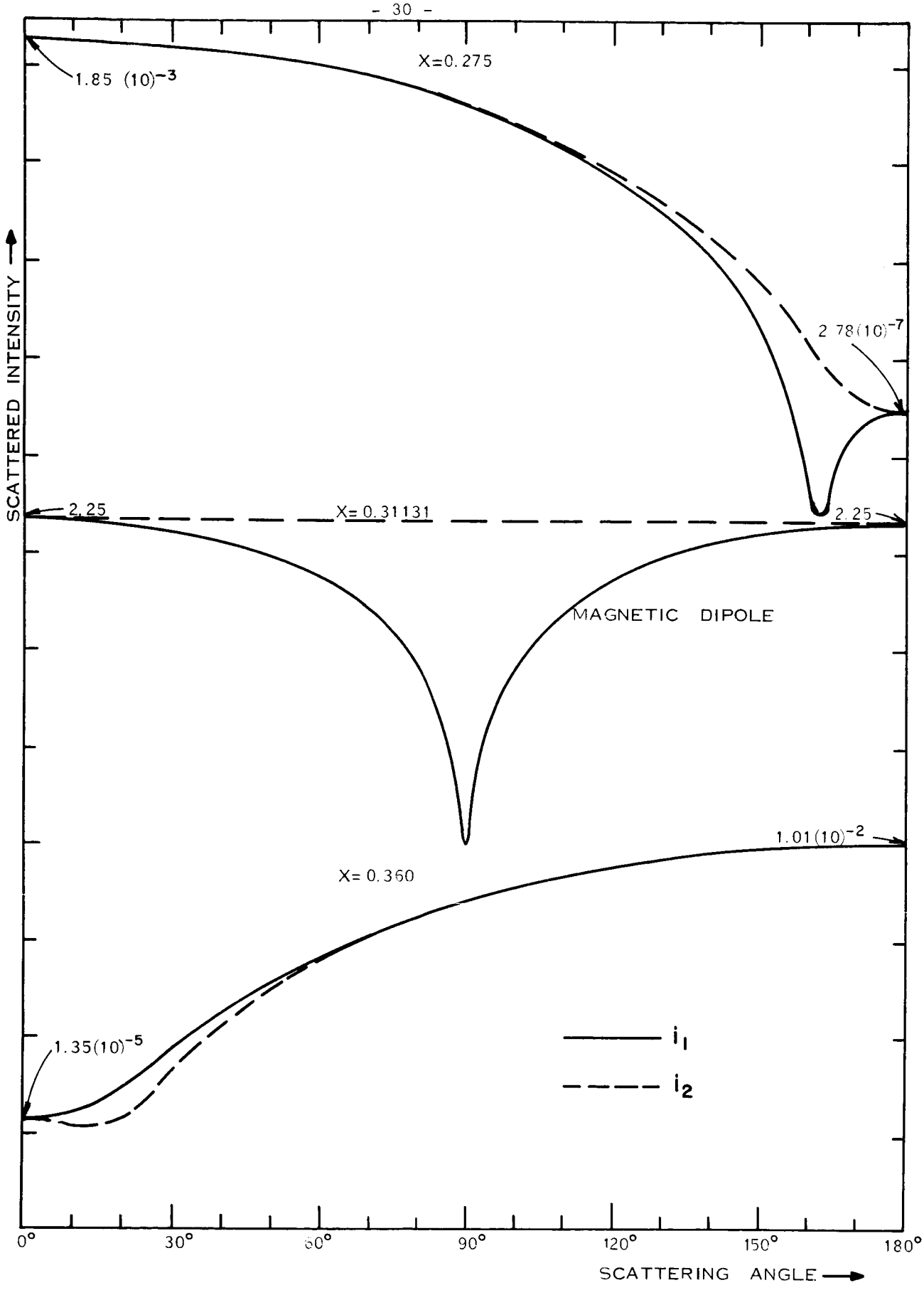
X=0.275
1.85 (10)$^{-3}$
2.78(10)$^{-7}$
SCATTERED INTENSITY
2.25
X= 0.31131
2.25
MAGNETIC DIPOLE
1.01(10)$^{-2}$
X= 0.360
1.35(10)$^{-5}$
i_1
i_2
0°
30°
60°
90°
120°
150°
180°
SCATTERING ANGLE

FIGURE 15

point, and the maximum backward scattering. When $x = 0.275$ the intensity functions i_1 and i_2 as defined by Van de Hulst[1] are 1.85×10^{-3} in the forward direction ($\theta = 0°$) and 2.78×10^{-7} in the backward direction ($\theta = 180°$). At the resonance point for magnetic dipole scattering $x = 0.31131$. The intensity i_2 is constant and equal to 2.25 to three significant figures at all angles; the intensity i_1 has a sharp minimum at 90° and is very nearly symmetrical about 90°. This is the Rayleigh scattering pattern expected for small values of x, except that the roles of i_1 and i_2 are reversed for magnetic dipole resonance scattering. When $x = 0.360$ the pattern has changed to strong backward scattering with an intensity of 1.35×10^{-5} at $\theta = 0°$ and 1.01×10^{-2} at $\theta = 180°$.

When $x < 0.1$ the intensity i_1 is nearly constant and i_2 has a sharp minimum near 90° as expected for Rayleigh scattering. As x increases the angular pattern is distorted by the magnetic dipole resonance as shown in Fig. 15. The higher multipoles similarly change the scattering pattern in a more and more complicated manner as the order of the multipole increases. The oscillations in $\langle \cos \theta \rangle_{av}$ near the first five multipoles are shown in Figs. 12 and 13. The actual angular distributions near these multipoles are so interesting that they are shown in Fig. 16. The angular distribution at the electric dipole resonance ($x = 0.44404$) is the same as for the magnetic dipole, except the roles of i_1 and i_2 are reversed.

The magnetic and electric quadrupole resonances at $x = 0.44775$ and $x = 0.57330$ respectively have similar angular intensity functions except for the interchange of i_1 and i_2. For the magnetic quadrupole, it is seen from Fig. 16 that the minimum of i_2 occurs at 90° and the minima of

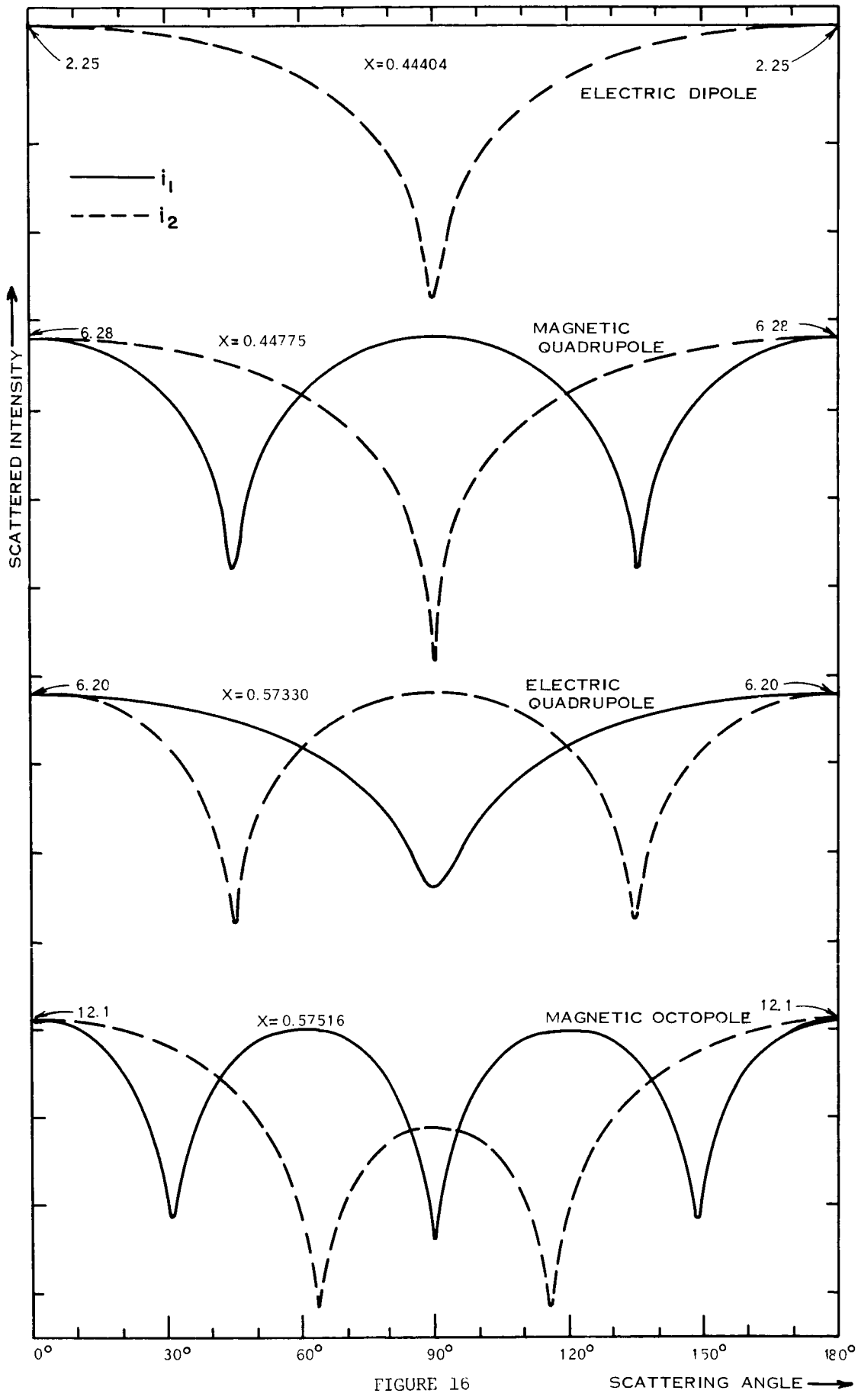
2.25
X=0.44404
2.25
ELECTRIC DIPOLE
i_1
i_2
SCATTERED INTENSITY
6.28
X=0.44775
MAGNETIC QUADRUPOLE
6.28
6.20
X=0.57330
ELECTRIC QUADRUPOLE
6.20
12.1
X=0.57516
MAGNETIC OCTOPOLE
12.1
0°
30°
60°
90°
120°
150°
180°
SCATTERING ANGLE

FIGURE 16

i_1 occur at 45° and 135°.

The magnetic octopole resonance at x = 0.57516 is also shown in Fig. 16. The following electric octopole resonance has a similar pattern with i_1 and i_2 interchanged. Calculation shows that the minima of i_1 occur at 31°5', 90°, and 148°55' and those of i_2 at 63°26' and 116°34'. All of these curves are very nearly symmetrical around 90°.

The general shape of these resonance scattering curves can readily be explained from the general equations for angular Mie scattering (e.g. p. 125 Van de Hulst[1]). At the magnetic dipole resonance the coefficient b_1 is much larger than any of the others. It follows from the equations that $i_1 \propto \cos\theta$ and i_2 = constant. This angular dependence is slightly modified by the other terms in the series with the result that i_1 is different from zero at $\theta = 90°$ and the distribution is very slightly asymmetric around $\theta = 90°$.

At the magnetic quadrupole resonance, the coefficient b_2 is dominant and the same equations show that $i_1 \propto \cos 2\theta$ and $i_2 \propto \cos\theta$. The observed pattern as shown in Fig. 16 follows from this dependence.

Similarly the coefficient b_3 dominates at the magnetic octopole resonance; thus $i_1 \propto \cos\theta + 15\cos 3\theta$ and $i_2 \propto 5\cos^2\theta - 1$. Again the observed angular pattern follows from these functions as slightly modified by the other terms in the summation. At resonance $\langle\cos\theta\rangle_{av}$ would be exactly zero, except for the contribution from other terms in the series. We have already remarked in connection with Fig. 14 that $\langle\cos\theta\rangle_{av}$ is zero for a value of x nearly equal to, but slightly different from the resonance value.

The electric multipole resonances occur when a coefficient a_n is dominant. The fundamental equations show immediately that the angular dependence is the same as for the magnetic multipole resonance for the same value of n as far as the contribution from the leading terms is concerned, provided the roles of i_1 and i_2 are interchanged. The actual curves may be somewhat different quantitatively, because of the contribution from other terms in the series. This can be seen by comparing the curves for the magnetic and electric quadrupole resonance shown in Fig. 16. The electric quadrupole resonance at 90° is broader and shallower than the corresponding curve for the magnetic quadrupole.

The angular intensity curves have been discussed in great detail for the case $n_1 = 10$ and $n_2 \approx 0$, because all of the resonances considered here occur at a value of $x < 1$. Thus, the additional effects due to interference between the various reflected and refracted rays which are introduced when $x > 1$ are avoided. However, the angular variation at the resonance points is qualititively the same for <u>any</u> non-absorbing sphere.

One can better understand the angular variation for moderate values of n_1 by thinking of the superposition of the angular patterns discussed here on the patterns caused by interference between the various reflected and refracted rays. For example, the angular patterns for $n_1 = 2$ are given on p. 152 of Van de Hulst[1]. When $x = 1$, the curves are those expected for Rayleigh scattering. At $x = 1.5$, the magnetic dipole resonance at $x = 2.2$ modifies the curves and they look like the upper set in Fig. 15.

At $x = 2$ and $x = 2.5$, i_1 is less than i_2 at almost all angles. Calculation shows that the expected resonance scattering curve (similar to the middle curves in Fig. 15) occurs at the resonance. The additional wiggles in these curves are caused by the superposition of the interference effects mentioned previously on the resonance scattering.

The magnetic dipole resonance occurs at the smallest value of x of any resonance. After this the resonances occur in pairs. The electric multipole resonance of order n-1 always occurs at a slightly smaller value of x than the magnetic multipole resonance of order n. The half-width of the resonances becomes narrower as the order increases and can easily be missed unless very fine intervals are taken in the calculations.

Strong forward scattering occurs on one side of a resonance and strong backward scattering on the other side. This effect may be obscured by other factors for high multipole resonances, but is very prominent for the first few resonances. The scattering is very nearly symmetric around 90° at the resonance.

Half-width of Angular Intensity Function

The angular intensity functions for the two directions of polarization $i_1(\theta)$ and $i_2(\theta)$ (as defined by Van de Hulst[1]) have their maximum values in the forward direction, $\theta = 0°$, in most cases. The only exception is when x is small and n_2 is large. Whenever $x >> 1$, there is a strong maximum in the forward scattering. This maximum becomes stronger and sharper as x increases and is largely due to diffraction effects from the scattering sphere. Thus the half-width of the intensity maximum should

be proportional to x^{-1} when $x>>1$. The actual variation of this half-width as a function of x, n_1, and n_2 has not been reported previously.

A computer program was developed which searched for the value of nearest 0° that resulted in a value of i_2 (θ) equal to one-half the value of i_2 (0°). The functions i_1 and i_2 are equal at $\theta = 0°$ and are nearly equal near the forward direction. The half-widths calculated from either of these functions were identical on the scale of these graphs, except in a few cases when $x << 1$. Since we are primarily interested in the half-widths for large values of x, only the results calculated from i_2 are shown.

In Fig. 17 the half-width in degrees is plotted as a function of x for $n_2 = 0$ and various values of n_1. When $x << 1$, the half-width is nearly 45° in all cases. As x increases, the half-width starts to decrease around $x = 1$. The half-width is nearly proportional to x^{-1} when $x>>1$; this indicates that the principal cause of the strong forward scattering for this range of x is diffraction effects by the sphere. There are moderate variations in the curves as n_1 is varied, but the general similarity of all the curves is a noteworthy feature.

The dependence of the half-width on n_2 is shown in Figs. 18 and 19. Again the curves show that the half-width is nearly proportional to x^{-1} whenever $x>>1$. The changes in the half-width as n_2 is varied between zero and unity are surprisingly small. From these results it is possible to estimate the extent of the forward scattering with considerable precision.

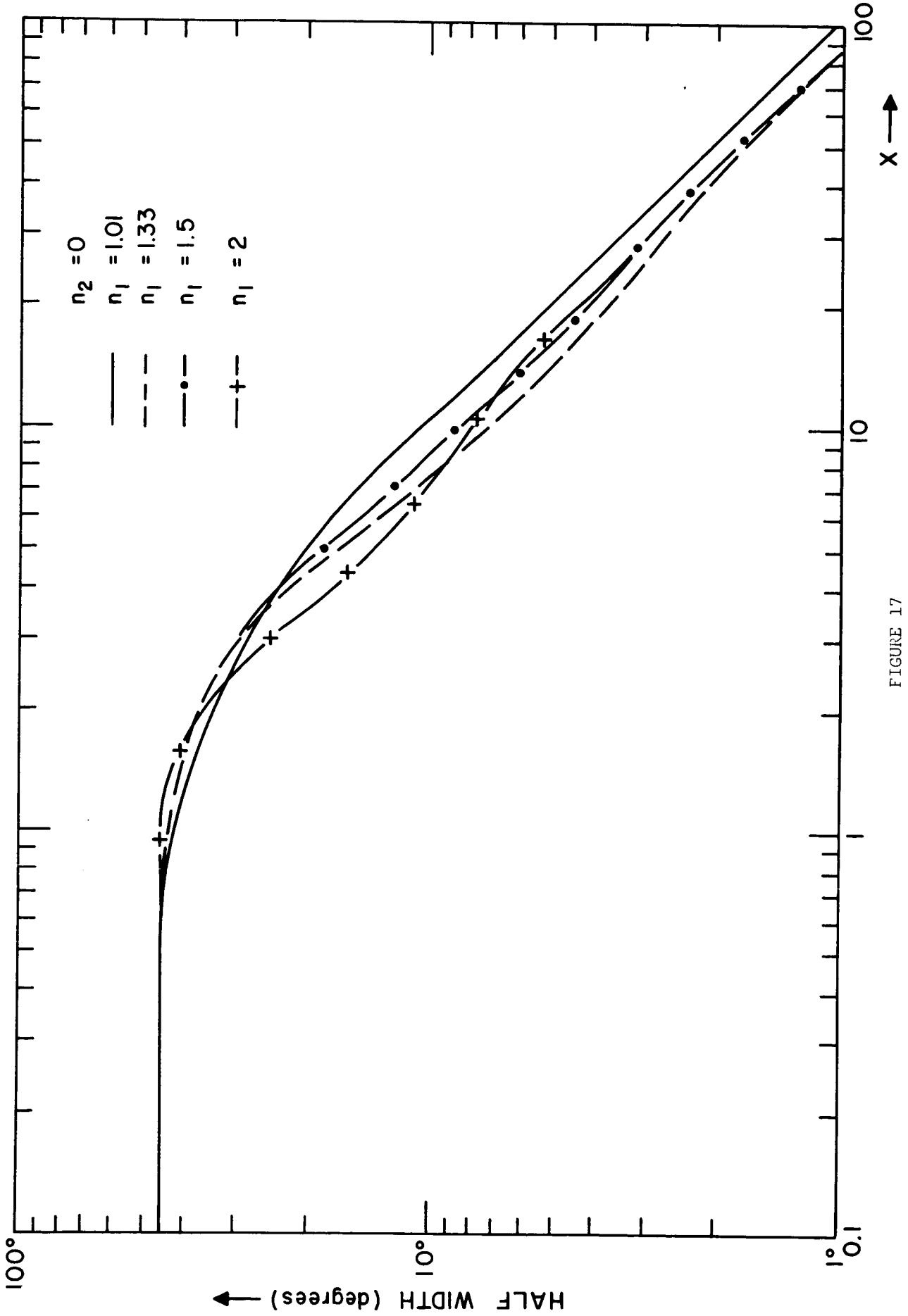
HALF WIDTH (degrees)
100°
10°
1°
0.1
100
10
1
X
n_2 =0
n_1 =1.01
n_1 =1.33
n_1 =1.5
n_1 =2

FIGURE 17

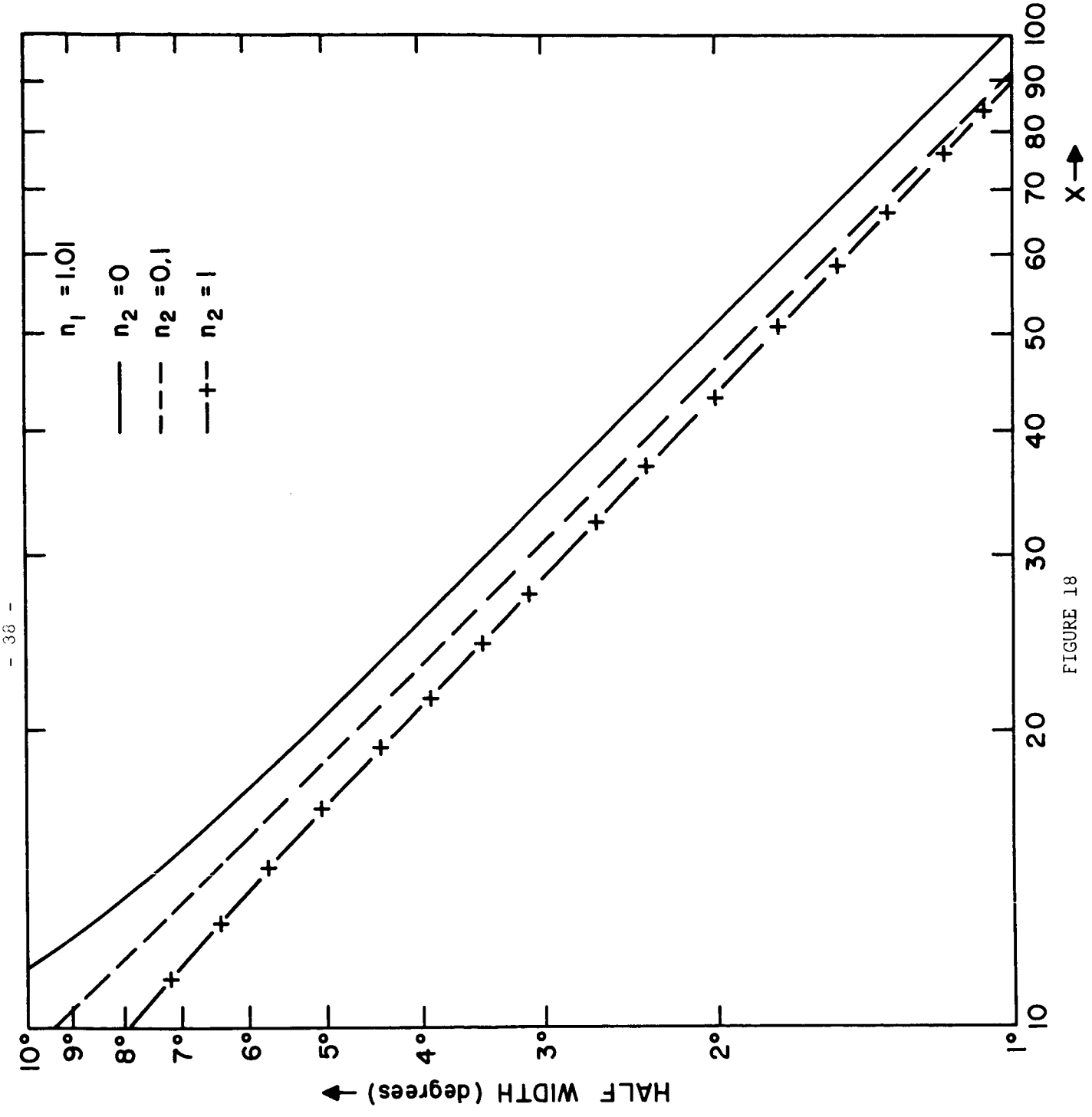
$n_1 = 1.01$
$n_2 = 0$
$n_2 = 0.1$
$n_2 = 1$
HALF WIDTH (degrees) ←
10°
9°
8°
7°
6°
5°
4°
3°
2°
1°
10
20
30
40
50
60
70
80
90
100
X →

FIGURE 18

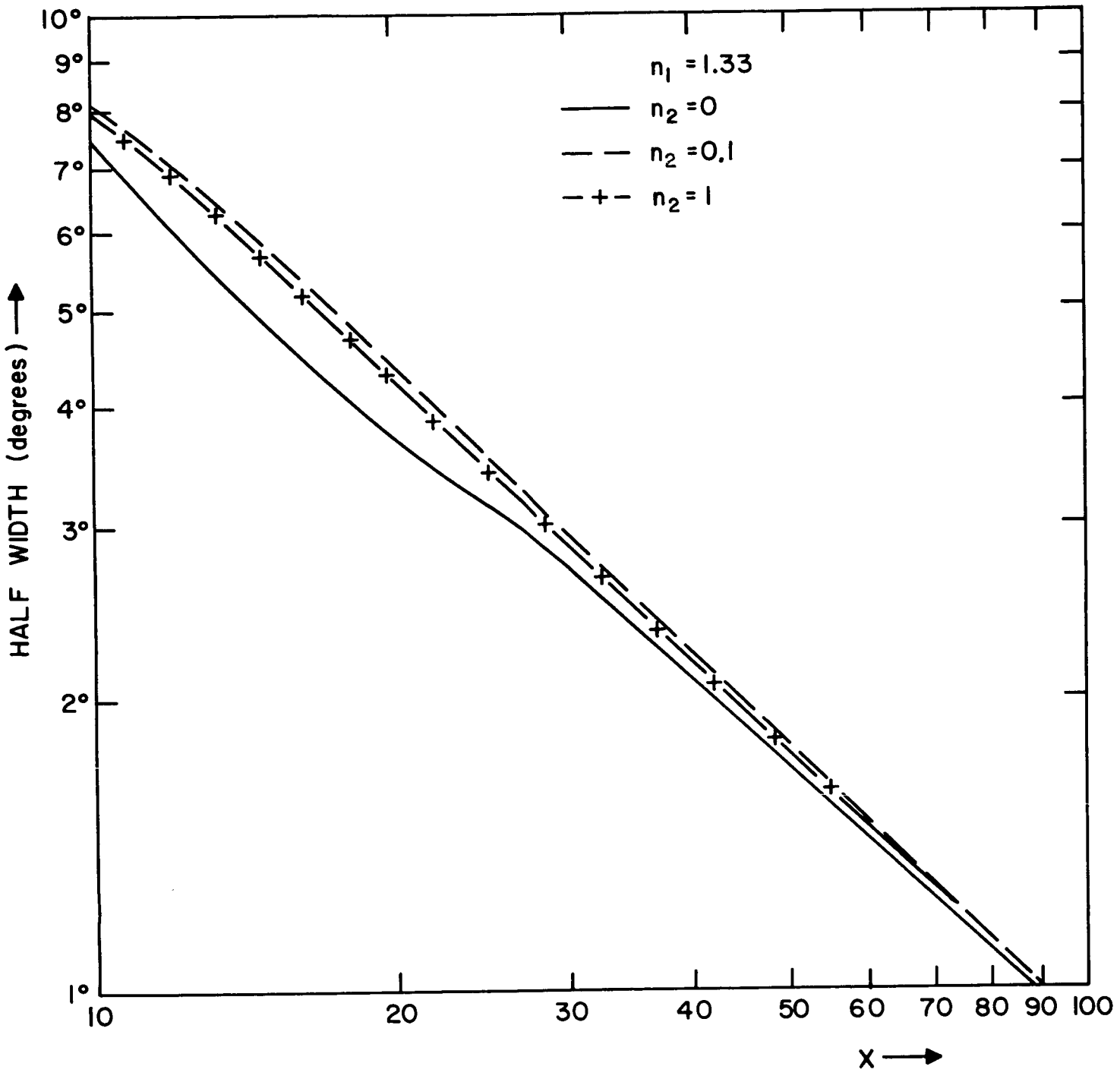
10°
9°
8°
7°
6°
5°
4°
3°
2°
1°
HALF WIDTH (degrees)
$n_1 = 1.33$
$n_2 = 0$
$n_2 = 0.1$
$n_2 = 1$
10
20
30
40
50
60
70
80
90
100
X

FIGURE 19

References

1. H. C. Van de Hulst, Light Scattering by Small Particles (Wiley, New York, 1957).
2. D. Deirmendjian, R. Clasen, and W. Viezee, J. Opt. Soc. Am. 51, 620 (1961).
3. A. Brockes, Optik 21, 550 (1964).
4. G. N. Plass, Appl. Opt. 5, 279 (1966).
5. A. L. Aden, J. Appl. Phys. 22, 601 (1951).
6. F. T. Corbato and T. L. Uretsky, J. Assoc. for Computing Machinery 6, 366 (1959).
7. R. H. Giese, Z. Astrophy., 51, 119 (1961).
8. P. J. Wyatt, Phys. Rev. 127, 1837 (1962).
9. L. Infeld, Quart. Appl. Math., 5, 113 (1947).
10. W. M. Irvine, J. Opt. Soc. Amer. 55, 16 (1965).

Captions for Figures

Fig. 1. Efficiency factor for absorption as a function of n_2 for $x = 2\pi a/\lambda = 0.1$ and various values of n_1.

Fig. 2. Efficiency factor for absorption as a function of n_2 for $x = 1$ and various values of n_1.

Fig. 3. Efficiency factor for absorption as a function of n_2 for $x = 10$ and various values of n_1.

Fig. 4. Efficiency factor for scattering as a function of n_2 for $x = 0.1$ and various values of n_1.

Fig. 5. Efficiency factor for scattering as a function of n_2 for $x = 1$ and various values of n_1.

Fig. 6. Efficiency factor for scattering as a function of n_2 for $x = 10$ and various values of n_1.

Fig. 7. Maximum value of Q_{ext} at the first resonance as a function of n_1 for various values of n_2.

Fig. 8. Width at half-maximum (in units of x) as a function of n_1 for various values of n_2.

Fig. 9. Average value of the cosine of the scattering angle as a function of n_2 for $x = 0.1$ and various values of n_1.

Fig. 10. Average value of the cosine of the scattering angle as a function of n_2 for $x = 1$ and various values of n_1.

Fig. 11. Average value of the cosine of the scattering angle as a function of n_2 for $x = 10$ and various values of n_1.

Fig. 12. Average value of the cosine of the scattering angle and Q_{ext} as a function of x for $n_1 = 10$ and $n_2 = 0$. The scales for the cosine and for Q_{ext} are on the left and right respectively.

Fig. 13. Average value of the cosine of the scattering angle and Q_{ext} as a function of x for $n_1 = 10$ and $n_2 = 0$ in the vicinity of the second and third resonances. The scales for the cosine and for Q_{ext} are on the left and right respectively.

Fig. 14. Average value of the cosine of the scattering angle as a function of the size parameter x for $n_1 = 10$ and 100. These values of x are in the immediate neighborhood of the first resonance in Q_{ext}.

Fig. 15. The scattered intensity as a function of the scattering angle for x = 0.275, 0.31131, and 0.360 and $n_1 = 10$, $n_2 = 0$. The values of the intensity at 0° and 180° are indicated above the curves near each margin. The solid curve is the intensity i_1 (as defined by Van de Hulst[1]) and the dashed curve is the intensity i_2. The logarithm of the intensity is plotted; each division indicated on this scale represents a factor of ten.

Fig. 16. The scattered intensity as a function of the scattering angle for x = 0.44404, 0.44775, 0.57330, and 0.57516 which corresponds to the electric dipole, magnetic quadrupole, electric quadrupole, and magnetic octopole resonances respectively and for $n_1 = 10$, $n_2 = 0$. See legend for Fig. 15.

Fig. 17. Half-width of angular intensity function in degrees as a function of size parameter x for $n_2 = 0$.

Fig. 18. Half-width of angular intensity function in degrees as a function of size parameter x for $n_1 = 1.01$.

Fig. 19. Half-width of angular intensity functions in degrees as a function of size parameter x for $n_1 = 1.33$.

14. KEY WORDS	LINK A		LINK B		LINK C	
	ROLE	WT	ROLE	WT	ROLE	WT
Electromagnetic scattering						
Absorbing spheres						
Mie Scattering						

INSTRUCTIONS

1. ORIGINATING ACTIVITY: Enter the name and address of the contractor, subcontractor, grantee, Department of Defense activity or other organization *(corporate author)* issuing the report.

2a. REPORT SECURITY CLASSIFICATION: Enter the overall security classification of the report. Indicate whether "Restricted Data" is included. Marking is to be in accordance with appropriate security regulations.

2b. GROUP: Automatic downgrading is specified in DoD Directive 5200.10 and Armed Forces Industrial Manual. Enter the group number. Also, when applicable, show that optional markings have been used for Group 3 and Group 4 as authorized.

3. REPORT TITLE: Enter the complete report title in all capital letters. Titles in all cases should be unclassified. If a meaningful title cannot be selected without classification, show title classification in all capitals in parenthesis immediately following the title.

4. DESCRIPTIVE NOTES: If appropriate, enter the type of report, e.g., interim, progress, summary, annual, or final. Give the inclusive dates when a specific reporting period is covered.

5. AUTHOR(S): Enter the name(s) of author(s) as shown on or in the report. Enter last name, first name, middle initial. If military, show rank and branch of service. The name of the principal author is an absolute minimum requirement.

6. REPORT DATE: Enter the date of the report as day, month, year; or month, year. If more than one date appears on the report, use date of publication.

7a. TOTAL NUMBER OF PAGES: The total page count should follow normal pagination procedures, i.e., enter the number of pages containing information.

7b. NUMBER OF REFERENCES: Enter the total number of references cited in the report.

8a. CONTRACT OR GRANT NUMBER: If appropriate, enter the applicable number of the contract or grant under which the report was written.

8b, 8c, & 8d. PROJECT NUMBER: Enter the appropriate military department identification, such as project number, subproject number, system numbers, task number, etc.

9a. ORIGINATOR'S REPORT NUMBER(S): Enter the official report number by which the document will be identified and controlled by the originating activity. This number must be unique to this report.

9b. OTHER REPORT NUMBER(S): If the report has been assigned any other report numbers *(either by the originator or by the sponsor)*, also enter this number(s).

10. AVAILABILITY/LIMITATION NOTICES: Enter any limitations on further dissemination of the report, other than those imposed by security classification, using standard statements such as:

(1) "Qualified requesters may obtain copies of this report from DDC."

(2) "Foreign announcement and dissemination of this report by DDC is not authorized."

(3) "U. S. Government agencies may obtain copies of this report directly from DDC. Other qualified DDC users shall request through _____."

(4) "U. S. military agencies may obtain copies of this report directly from DDC. Other qualified users shall request through _____."

(5) "All distribution of this report is controlled. Qualified DDC users shall request through _____."

If the report has been furnished to the Office of Technical Services, Department of Commerce, for sale to the public, indicate this fact and enter the price, if known.

11. SUPPLEMENTARY NOTES: Use for additional explanatory notes.

12. SPONSORING MILITARY ACTIVITY: Enter the name of the departmental project office or laboratory sponsoring *(paying for)* the research and development. Include address.

13. ABSTRACT: Enter an abstract giving a brief and factual summary of the document indicative of the report, even though it may also appear elsewhere in the body of the technical report. If additional space is required, a continuation sheet shall be attached.

It is highly desirable that the abstract of classified reports be unclassified. Each paragraph of the abstract shall end with an indication of the military security classification of the information in the paragraph, represented as *(TS), (S), (C), or (U)*.

There is no limitation on the length of the abstract. However, the suggested length is from 150 to 225 words.

14. KEY WORDS: Key words are technically meaningful terms or short phrases that characterize a report and may be used as index entries for cataloging the report. Key words must be selected so that no security classification is required. Identifiers, such as equipment model designation, trade name, military project code name, geographic location, may be used as key words but will be followed by an indication of technical context. The assignment of links, rules, and weights is optional.

Unclassified

Security Classification

DOCUMENT CONTROL DATA - R&D

(Security classification of title, body of abstract and indexing annotation must be entered when the overall report is classified)

1. ORIGINATING ACTIVITY (Corporate author)
Southwest Center for Advanced Studies
Dallas, Texas 75230

2a. REPORT SECURITY CLASSIFICATION
Unclassified

2b. GROUP

3. REPORT TITLE
ELECTROMAGNETIC SCATTERING FROM ABSORBING SPHERES

4. DESCRIPTIVE NOTES (Type of report and inclusive dates)
Interim Scientific Report

5. AUTHOR(S) (Last name, first name, initial)
Kattawar, George W.
Plass, Gilbert N.

6. REPORT DATE	7a. TOTAL NO. OF PAGES	7b. NO. OF REFS
28 December 1966	45	10

8a. CONTRACT OR GRANT NO.
AF19(628)-5039
b. PROJECT and Task No.
4076-04
c. DoD Element No.
62405484
d. DoD Subelement No. 634076

9a. ORIGINATOR'S REPORT NUMBER(S)
Scientific Report No. 1

9b. OTHER REPORT NO(S) (Any other numbers that may be assigned this report)
AFCRL-67-0129

10. AVAILABILITY/LIMITATION NOTICES
DISTRIBUTION OF THIS DOCUMENT IS UNLIMITED

11. SUPPLEMENTARY NOTES partially supported by the National Aeronautics and Space Administration

12. SPONSORING MILITARY ACTIVITY
Hq. AFCRL, OAR (CRO)
United States Air Force
L.G.Hanscom Field, Bedford,Mass. 01730

13. ABSTRACT

A very efficient method for the calculation of Mie cross sections for absorbing particles is discussed. It is used to calculate an extensive set of curves which illustrate the dependence of the efficiency factors Q for absorption, scattering, and extinction on the size parameter x and on n_1 and n_2 (the real and imaginary parts of the index of refraction). Other curves show the height and width of the first resonance in Q_{ext} as a function of x as well as the average cosine of the scattering angle and the half-width of the angular intensity function as it depends on x, n_1, and n_2. Among the interesting features shown are the following: (1) as n_2 increases, Q_{sca} decreases to a minimum value before increasing, when $x \geq 1$ and for most values of n_1; (2) the maximum value of Q_{ext} at the first resonance decreases rapidly when a small amount of absorption is introduced; (3) over a considerable range of the parameters the width of the first resonance of Q_{ext} is proportional to n_1^{-4} when there is no absorption and to $n_2 n_1^{-2}$ when there is absorption; (4) when $n_1 >> 1$, the scattered intensity near the first resonance is predominately forward, symmetrical, or predominately backward when x is respectively somewhat smaller than, equal to, or larger than the the resonance value; (5) as n_2 increases, the forward scattered intensity first increases before it decreases, when $x \geq 1$ and for most values of n_1; (6) the half-width of the angular intensity function varies as x^{-1} when $x \geq 10$ and is relatively insensitive to the value of n_1 and n_2.

DD FORM 1 JAN 64 1473

Unclassified

Security Classification